AD

AD-E404 351

Technical Report ARMET-TR-20022

MODELING THE ADHESION OF EPOXY TO ALUMINUM AND THEIR SEPARATION UNDER DYNAMIC LOADS USING ABAQUS AND LS-DYNA

Catherine S. Florio

February 2022

U.S. ARMY COMBAT CAPABILITIES DEVELOPMENT COMMAND ARMAMENTS CENTER

Munitions Engineering Technology Center

Picatinny Arsenal, New Jersey

The views, opinions, and/or findings contained in this report are those of the author(s) and should not be construed as an official Department of the Army position, policy, or decision, unless so designated by other documentation.

The citation in this report of the names of commercial firms or commercially available products or services does not constitute official endorsement by or approval of the U.S. Government.

Destroy by any means possible to prevent disclosure of contents or reconstruction of the document. Do not return to the originator.

All results derived from computer simulations are bound by the technical assumptions made during the creation of the models used to generate said simulations. The FCDD-ACM-AA personnel cannot be held responsible for deviations that may occur as a result of technical parameters beyond, or not covered by, the originally agreed upon scope of work. Any values generated by use of computer simulation should be validated through live-fire testing prior to publishing the data in an uncontrolled environment.

REPORT DOCUMENTATION PAGE	*Form Approved OMB No. 0704-01-0188*

1. REPORT DATE (DD-MM-YYYY)	2. REPORT TYPE	3. DATES COVERED (*From - To*)
February 2022	Final	January 2019 - September 2019

4. TITLE AND SUBTITLE	5a. CONTRACT NUMBER
Modeling the Adhesion of Epoxy to Aluminum and Their Separation under Dynamic Loads using Abaqus and LS-DYNA	5b. GRANT NUMBER
	5c. PROGRAM ELEMENT NUMBER
6. AUTHORS	5d. PROJECT NUMBER
Catherine S. Florio	5e. TASK NUMBER
	5f. WORK UNIT NUMBER

7. PERFORMING ORGANIZATION NAME(S) AND ADDRESS(ES)	8. PERFORMING ORGANIZATION REPORT NUMBER
U.S. Army DEVCOM AC, METC Armaments Engineering Analysis and Manufacturing Directorate (FCDD-ACM-AA) Picatinny Arsenal, NJ 07806-5000	
9. SPONSORING/MONITORING AGENCY NAME(S) AND ADDRESS(ES)	10. SPONSOR/MONITOR'S ACRONYM(S)
U.S. Army DEVCOM AC, ESIC Knowledge & Process Management Office (FCDD-ACE-K) Picatinny Arsenal, NJ 07806-5000	11. SPONSOR/MONITOR'S REPORT NUMBER(S) Technical Report ARMET-TR-20022

12. DISTRIBUTION/AVAILABILITY STATEMENT
Approved for public release; distribution is unlimited.

13. SUPPLEMENTARY NOTES

14. ABSTRACT

The modeling of adhered surfaces and the prediction of their separation within multicomponent systems is not widely used in the study of armament systems. Approximations commonly made to bound the problem add to the uncertainty of the predicted results and conclusions drawn about the integrity of the system, particularly under highly dynamic load environments. The use of adhesive/cohesive interface models in systems where either a thin film or large bulk volume of epoxy is bonded to an aluminum substrate is investigated in this work. Both quasi-static and highly dynamic loading conditions are considered, with the accelerations varying over three orders of magnitude. The influence of interface model parameters such as adhesive strength, damage evolution models, and comparisons to simple frictional interface models are evaluated. The influence of mesh and geometric simplifications are also discussed, and predictions in two commonly used commercial finite element codes, Abaqus and LS-DYNA, are compared. Recommendations are made regarding the relative sensitivity of predicted results on interface model types and parameters used over the range of loading conditions studied.

15. SUBJECT TERMS
Cohesive zone modeling Interface models Dynamic loads Epoxy Aluminum
Finite element modeling

16. SECURITY CLASSIFICATION OF:			17. LIMITATION OF ABSTRACT	18. NUMBER OF PAGES	19a. NAME OF RESPONSIBLE PERSON
a. REPORT	b. ABSTRACT	c. THIS PAGE			Catherine S. Florio
U	U	U	SAR	43	19b. TELEPHONE NUMBER (Include area code) (973) 724-8267

Standard Form 298 (Rev. 8/98)
Prescribed by ANSI Std. Z39.18

CONTENTS

FIGURES

FIGURES
(continued)

Page

ACKNOWLEDGMENTS

This work was funded by a Modeling and Simulation Advanced Initiatives Project of the U.S. Army Combat Capabilities Development Command Armaments Center, Picatinny Arsenal, NJ, Modeling and Simulation Strategic Advisory Group.

INTRODUCTION

The adhesion of significantly disparate materials is commonly used in a wide range of systems from joints bonded with adhesives (refs. 1 through 4) to coatings (ref. 5) to barnacles and other fouling marine organisms on shipping vessels (ref. 6). The quasi-static tensile adhesive strength is often of most importance since many of these applications involve a thin coating of the adhesive. In these situations, pull or peel tests are often performed as a means to gage interface strength (refs. 4 and 6 through 9). When systems are subjected to highly dynamic loads, when adhesive layers are relatively thick compared to the adherents, or when loading modes involve shear in addition to or instead of tensile forces, such standard methods for assessing adhesive strength are no longer applicable, and other means to estimate conditions that induce failure of the bonded interface are required (refs. 7 through 12). Further, when these adhered interfaces are a small part of a much larger system and when the overall system response, rather than that of the adhered joint itself, is of interest, it is not always possible to specifically characterize the interface behavior. As a result, estimates of the interface behavior are made, often through the application of frictional interface models to represent a failed adhesive or a fully bonded interface model to represent an adhered interface (refs. 7, 8, and 11 through 13). However, it has been shown that the use of friction and contact models do not appropriately capture the behavior in many conditions between initially adhered interfaces. It has been shown that the transitions between adhered, failing, and fully separated states of an interface, including the resulting energy losses, must be well represented in order to properly predict the effect that they may have on the overall system behavior as well as that of the neighboring components (refs. 11, 12, and 14). The intent of this study is to examine the differences in the prediction of the behavior of a representative system of an epoxy-filled metal housing that is subjected to an impact load when using different interface model types and parameter values. The insight gained from this study can guide the selection of an appropriate level of detail in the interface model used for a particular application.

The importance of incorporating a model that well represents the interface behavior between an adhesive and adherent, such as an epoxy and a metal, has been shown in a number of studies, particularly as the thickness and mass of the adhesive increases and the load acting on the system becomes more transient. In an examination of the behavior of a polymer epoxy-based explosive that fills the interior of a large caliber munition, it was found that the use of a friction model at the initially adhered interface between the epoxy explosive and an aluminum shell could not accurately predict the deformation in the explosive within a munition that was seen through X-rays taken during an experimental gun launch event (ref. 12). Even with an improved constitutive model of the material properties of the explosive, the simulation could not predict the deformed shapes seen in the X-rays, particularly the concave geometry that results on the faces with surface normals that are initially parallel to the direction of the acceleration (ref. 11). The authors of reference 11 concluded that the observed concave shape was a result of the movement of the bulk material of the epoxy-based explosive in the direction of motion due to the inertial force, which is resisted by the chemical and mechanical adhesion at its interface with the metal shell. They concluded that the discrepancy between the simulation and experimental observation showed that the interaction between the initially adhered components was not negligible compared to their bulk behaviors, even under the inertial loads induced in gun launch. Therefore, a computational model that includes a proper representation of the adhesion and failure of that adhered interface in addition to the improved material model would be needed to properly predict the experimentally observed system behavior.

This conclusion was also made in the study of the adhesive strength of an “elastomeric potting material” that is often used to encapsulate or surround sensitive electronic components in order to damp vibrations or other loads, such as what may occur due to impact loads (refs. 7 and 8). The concern of this study was the stresses that are induced in the electronic components adhered to the epoxy material due to its expansion and contraction as a result of environmental temperature changes. In a series of studies, the author examined the sensitivity of interface model types and

parameters on the prediction of adhered interface behavior under quasi-static tensile and shear loads. In these studies, thin layers of epoxies were sandwiched between aluminum plates. The progressive separation behavior between these layers that was observed experimentally was able to be replicated computationally with the proper selection of model parameters. However, the authors noted a “considerable uncertainty in the calibration of the traction-separation model parameters developed” (ref. 7) in their work.

The studies reviewed indicate that while the inclusion of adhesive interface models may be important to capture system behaviors that are influenced by changes in the integrity of these bonds, the ability to properly predict this behavior can be difficult. A number of modeling methods have been developed to study adhesives, adhered joints, and their failures. There are three main ways to study interface behavior: (1) through local constitutive material models, (2) through local interface models, and (3) through bulk effects of adhesion models (ref. 14). Material constitutive models simulate the adhesive behavior with customized elastic-plastic models and can involve fracture, damage, or other failure models. They are applied through volume (area) elements that have mass. However, these often require extensive material testing to obtain the information required to identify the appropriate material model parameters and coefficients. Interface models are implemented through zero-mass/zero-thickness surface elements. They relate the normal and shear traction at the interface to the relative motion/separation of the adhered surfaces in a similar way to that of contact models for non-adhered interface interactions. Local interface models can include additional functions to predict the work of the progressive interface failure/debonding and associated separation as well as the energy dissipation that result from the separation (ref. 13). These energy changes are incorporated into the constitutive material model in a similar way to that of the transient energy dissipation due to material failure. Because of the similarity to contact, the adhesive interface models have the benefit of being able to directly convert to contact/friction interface models as the surfaces separate. Finally, bulk behavior models integrate the local behavior over the areas of the contacting surfaces to address the potentially multiple scales over which the adhesive behaviors can act, such as the effects of surface roughness, intermolecular forces, and microstructures.

For the loading environment of interest in the current work, the effects of shear forces in addition to normal tractions exist at the interface between the volume of epoxy and its metal shell container. While the adhered surfaces in the system studied are a small, relatively uncharacterized component of a larger system, the mass of the adhesive itself is of significant mass in comparison to the other system components. As a result, local interface models were the focus of the current investigation.

Previous experimental studies have examined the effects of the relative size of the adhesive layer compared to the overall system and of the loading conditions on the interface strength. A study was performed examining the tensile strength as a function of diameter of the adhered region, modulus of the adhesive, and thickness of the adhesive layer (ref. 6). When the thickness of the adhesive was much larger than the radius of the adhered region, the adhesive strength was proportional to the square root of the ratio of the adhesive modulus to the radius of the adhered region. In contrast, when the thickness of the adhesive was much smaller than the radius of the adhered region, this measure was proportional to the square root of the ratio of the elastic modulus to the thickness, indicating an increased influence of adhesive thickness. In a similar study, the effect of adhesive thickness, adhesive modulus, and loading shear rate on the shear strength of the interface between an aluminum plate and a coating of Loctite was investigated (ref. 5). It was found that for low modulus adhesive, on the order of 0.1 MPa, the shear stress at the interface increased significantly with decreasing adhesive thickness, as less energy was used to deform the relatively compliant adhesive. With the thinner coatings, the shear rate studied, on the order of 10 microns/s, also had a noticeable effect on the shear stress. However, as the modulus of the adhesive increased to be on the order of 1.0 MPa, the shear rate and thickness effects were no longer significant, though greater loads were required to cause failure at the adhered interface than for the lower modulus

adhesives for equal material thickness and load rates. Finally, this study showed that under higher strain rates, such as those due to impact, on the order of 100 s^{-1} , the adhesive shear strength was shown to increase with increasing strain rates over the adhesive strength measured under quasi-static conditions.

In each of these experimentally studied systems, the conditions under which an interface fails vary based on the characteristics of the system. Therefore, an understanding of the relationships between the system conditions and the interface behavior becomes important to the proper prediction of the separation of initially adhered surfaces using computational models. Some studies have been previously performed to understand the limitations of the interface modeling methods that were used to predicting interface separation behavior. In an investigation of the failure of single-lap joints, it was found that interface model that was used effectively predicted the system behavior for brittle or moderately ductile adhesives but not for adhesives that resulted in significant plasticization before failure (ref. 2). The authors of this study concluded that in such cases, the failure occurs in the bulk of the adhesive, not at the interface, and, therefore, without modeling the adhesive explicitly, such behavior and damage could not be predicted. Other studies have shown that the type of softening law used in the damage model did not have a significant influence on the predictions of interface failure when the adhesive thickness was small compared to the component length scale (ref. 3). This corresponds with the experimentally observed behavior regarding the effect of adhesive thickness on interface strength and energy dissipation during separation of adhered surfaces that was discussed earlier in this review.

Studies such as the ones described can be helpful to guide both the selection of adhesives for particular applications and the development of computational models to predict their behavior. Often, computational models require the experimental determination of parameters which are used as part of the material or interface behavior models. Despite the significant information available on the system conditions and parameters that may influence adhesive interface strength, which can be used to direct the experimental studies that obtain these parameter values, for many design applications, particularly where the interface is not the focus of the design, the experimental determination of model parameters, even for built-in routines, may not be feasible. As a result, the adhesive interface is often ignored, and simply fully bonded or fully separated, frictionless, interface conditions are examined to “bound” the problem at the two potential extremes. These two extremes induce different interactions, from local stressing of bonded interfaces being pulled from each other to impact between components free to slide, unrestrained, within a system. This can cause a challenge in making design decisions, especially as design limits are approached and safety factors are small.

As described in this brief review, to obtain a better estimate of the interface behavior between initially adhered surfaces, particularly if separation between them cannot be excluded under the conditions studied, the strength of the adhered interface, the energy release from its separation, the change in behavior with time as the bond is gradually broken, must be included. The phenomena modeled must include the reduction in bond length and the new interface behavior that begins, such as sliding friction, contact, or rebonding. Further, while the reviewed work does examine the effects of the system and loading parameters, such as load rate, adhesive thickness, and adhesive stiffness, few studies have examined how well the values of these parameters must be known. Specifically, not well understood is the sensitivity of the adhesive model parameters used in a system where the mass of the adhesive has a significant contribution to the overall system mass and inertial effects are important to understanding interaction of initially adhered components under high-load rate conditions. With a focus on applications where the adhered interface is not being designed, though its behavior influences the function of the system that is being designed, this study examines built-in interface model features of LS-DYNA and Abaqus. The sensitivity of the predicted system behavior to the interface model parameters used, the influence of the use of an adhesive interface with interface damage and failure rather than a frictional or bonded interface model to transfer for tangential and normal loads between components, and the differences in the two software packages

will be explored. The focus will be on the system with initially fully bonded epoxy-to-aluminum interfaces within a system subjected to a range of transient loads.

METHODS

The work was performed in two main stages. In the first stage, the built-in cohesion/adhesion modeling capabilities of two commercial software packages, Abaqus and LS-DYNA, were used to simulate the quasi-static behavior under pure axial tension and under pure shear of two metal plates bonded through a layer of epoxy adhesive. The effect of the adhesive model parameters that were used was evaluated as the results of this study were compared to those in a previously published work (ref. 7). Once the adhesive model was validated for quasi-static conditions, it was then used to evaluate a system where a volume of adhesive material fills a cylindrical metal container and the system is subjected to a dynamic load. The effect of the load magnitude and failure parameters of adhesive interface model were studied. Comparisons of behavior to the use of a friction interface model were made. In addition, the behavior predicted by two commercial codes with the same set of system, loading, and interface model parameters were also compared for a range of loading magnitudes. Through these methods, a better understanding of the model parameters that most influence the predicted behavior of adhered interfaces under a range of conditions and of the benefits and limitations of currently available commercial codes is obtained. Abaqus CAE 2019 and LS-DYNA version R10.1.0 with LS-PrePort-4.6.1 were used in this work.

Material Models

The systems studied were comprised of two materials. The metal was aluminum and the adhesive was Sylgard. This combination followed a previously published study used for validation (ref. 7). The material models and properties used in this work are briefly presented. The same material models were used for both the quasi-static and the dynamic conditions examined.

Aluminum

The plates in the quasi-static study and the cylindrical canister in the dynamic study were made of aluminum 7075. A linearly elastic isotropic material model was used to represent the aluminum since failure and damage to the system was assumed to be solely at the interface with the adhesive. The model represented the aluminum with a density of 2,810 g/m^3, an elastic modulus of 71.7 GPa, and a Poisson's ratio of 0.3.

Sylgard (Epoxy)

The epoxy adhesive binding the aluminum plates in the quasi-static study and within the canister in the dynamic study was Sylgard, represented as an isotropic, hyperelastic, nearly incompressible rubber material. Following the previous work (ref. 7), the density of the adhesive used in this study was 1,030 g/m^3, the initial shear modulus, μ_0 , was 0.44 MPa, and the initial bulk modulus, k_0, was 1.214 GPa. The Poisson's ratio, ν, which represents the relative compressibility of this rubber, was found to be 0.4998 through the relation:

$$\nu = \frac{3\frac{k_0}{\mu_0}-2}{6\frac{k_0}{\mu_0}+2} \quad (1)$$

The material model used will be briefly explained and the implementation through built-in functions in the two commercial finite element codes used in this work, Abaqus and LS-DYNA, will be

presented (refs. 15 and 16). Following the previously published study that was used to validate the model created in this work, a neo-Hookean material model was employed.

The neo-Hookean material model describes the local strain energy density, Ψ, as a simplification of the polynomial series function of the scalar invariants, I_i , of the right Cauchy-Green strain tensor, **C**, at each point in the material in the following way:

$$\Psi(I_1, I_3) = c(I_1 - 3) + d(I_3 - 1)^2 \tag{2}$$

where *c* and *d* are material property constants and the invariants are written as:

$$I_1(\mathbf{C}) = tr(\mathbf{C}) \tag{3a}$$

$$I_2(\mathbf{C}) = \frac{1}{2}\left(\left(tr(\mathbf{C}^2)\right)^2 - tr(\mathbf{C}^2)\right) \tag{3b}$$

$$I_3(\mathbf{C}) = |\mathbf{C}| \tag{3c}$$

and. This form is valid for moderate stretches of the material where the strain does not exceed 100% (ref. 17).

For the isotropic conditions, the Cauchy-Green strain tensor is symmetric so that the invariants can then be written in terms of the eigenvalues of the tensor, or physically, the principal stretches, λ_i. As a result, the third invariant becomes the square of volumetric compression ratio, *J*.

$$I_3(\mathbf{C}) = |\mathbf{C}| = J^2 \tag{4}$$

Therefore, if the material is incompressible or nearly incompressible, the volumetric compression ratio approaches a value of one, so that the third invariant term in the strain energy density function form in equation 2 typically becomes negligible compared to the first invariant term. It is useful to decouple the dilatational and deviatoric behavior in order to create modified expressions of the invariants in equation 3, which are identified by the bar as, $\overline{I_i}$. The decoupled form of the strain energy density is in equation 5.

$$\Psi(\overline{I_1}, \overline{I_3}) = c(\overline{I_1} - 3) + d(\overline{I_3} - 1)^2 \tag{5}$$

These modified invariants correspond to modified principal stretches, $\overline{\lambda_i}$.

In finite element formulations, the separation of the dilatational and deviatoric effects is beneficial to the numerical solutions involving this constitutive model. Further, the approximation of an incompressible material with such a decoupled compressible formulation using a Poisson's ratio slightly less than 0.5 helps the numerical stability of this solution (ref. 17).

Such a form is used in the commercial code Abaqus (ref. 15) where the strain energy density function is of the form:

$$\Psi(\overline{I_1}, J) = \frac{\mu_0}{2}(\overline{I_1} - 3) + \frac{k_0}{2}(J - 1)^2 \tag{6}$$

where the volumetric compression ratio and the material properties can be functions of temperature.

For the material considered in this work, the Poisson's ratio was 0.4998, making the second term in equation 6 negligible. Thus, the strain energy density function for the material examined in this study is nearly a linear function of the modified first invariant of the strain tensor used.

$$\Psi(\bar{I}_1) \cong \frac{\mu_0}{2}(\bar{I}_1 - 3) \tag{7}$$

If two terms are held in the polynomial expansion of the isometric hyperelastic material instead of just one as in the neo-Hookean material model described previously, a Mooney-Rivlin model results. In the Mooney-Rivlin model, the effect of the second invariant is also considered, allowing for larger stretch (strain) magnitudes to be considered. This model is described as:

$$\Psi(I_1, I_2, I_3) = c_1(I_1 - 3) + c_2(I_2 - 3) + d(I_3 - 1)^2 \tag{8}$$

LS-DYNA does not have a built-in neo-Hookean model (ref. 16). However, it does have a built-in Mooney-Rivlin model with a small volumetric compression assumption. The specific form used in this software is:

$$\Psi(I_1, I_2, I_3) = A(I_1 - 3) + B(I_2 - 3) + C\left(\frac{1}{{I_3}^2} - 3\right) + D(I_3 - 1)^2 \tag{9}$$

where A, B, C, and D are material parameters such that $\mu_0 = 2(A + B)$, $C = 0.5A + B$, and D is a function of A, B, and the Poisson's ratio, ν. With a nearly incompressible material, the last two terms of equation 9 become negligible, and the material model is reduced to:

$$\Psi(I_1, I_2) = A(I_1 - 3) + B(I_2 - 3) \tag{10}$$

To obtain a material model that is nearly the same as the one used in the Abaqus neo-Hookean model described in equation 7, the parameters A and B can be selected so that:

$$\Psi(I_1, I_2) = (\frac{\mu_0}{2} - 1)(I_1 - 3) + 1(I_2 - 3) \tag{11}$$

With the magnitude of the shear modulus μ_0 of the studied epoxy material as defined in equation 11 as much larger than 1, it can be reduced to:

$$\Psi(I_1) = \frac{\mu_0}{2}(I_1 - 3) \tag{12}$$

Interface Model

Built-in surface-based cohesive models of two commercial codes (Abaqus and LS-DYNA) (refs. 15 and 16) were used in this work and the results compared. The general models used in each of these software will be briefly discussed. Specific parameters and features used in each of the cases studied will be presented with the description of the case.

The built-in cohesive interface function in Abaqus focuses on controlling the movement of slave nodes that are initially in contact for a predefined pair of surfaces. A surface traction is created to simulate the forces generated between the bonded surfaces upon loading. This traction is proportional to the strain at these surface nodes due to compliance in the adhesive material which is being simulated by the cohesive interface model. In this study, the interface is given independent normal and shear stiffnesses so that the traction separation rule in equation 13 results. In the following equations, the subscripts n, s, and t represent the normal component and the two shear components, respectively. The surface traction vector for the slave node at the adhered interface is $\mathbf{t}$, $\mathbf{K}$ is the stiffness matrix, and δ is a vector that describes the relative motion of the slave node from the master surface.

$$\begin{bmatrix} t_n \\ t_s \\ t_t \end{bmatrix} = \begin{bmatrix} K_{nn} & 0 & 0 \\ 0 & K_{ss} & 0 \\ 0 & 0 & K_{tt} \end{bmatrix} \begin{bmatrix} \delta_n \\ \delta_s \\ \delta_t \end{bmatrix} \tag{13}$$

Damage to the interface can be initiated through a number of criteria. The simplest, a maximum nominal stress, was used in the Abaqus models in this work (see eq. 14). In this equation, the superscript *0* indicates the traction of the user-input adhesive strength material property. Only tensile, not compressive, normal traction is considered. This is indicated by the brackets as in $\langle t_n \rangle$.

$$max\left\{\frac{\langle t_n \rangle}{t_n^0}, \frac{t_s}{t_s^0}, \frac{t_t}{t_t^0}\right\} = 1 \tag{14}$$

Once initiated, damage can evolve in a number of different ways. Damage is described as the rate in which the cohesive stiffness is degraded once the damage initiation criteria is reached. Thus, after the interface failure strength is reached, the traction at the interface surface in equation 13 is scaled from its peak value $\mathbf{t}_0$ by the damage parameter D as:

$$\mathbf{t} = (1 - D)\mathbf{t}_0 \tag{15}$$

The damage parameter D is equal to zero when no damage exists. It is equal to one when full damage occurs. The damage parameter is assigned to each node pair for nodes that are initially in contact at the adhered surface. The separation during the process of interface failure is then calculated based on this new degraded traction and the original interface stiffness. In the built-in features in Abaqus, the damage parameter D can be either a function of the displacement of the slave nodes relative to the master surface or a function of the energy at the failing interface. The relationship between the damage parameter and this measure of the interface state at each slave node can be linear or exponential. Because there is compliance at the interface through equation 13, there is a certain amount of separation of the adhered surfaces that can occur before the damage is initiated. The separation after this threshold value then progresses while producing increasing amount of damage until the interface is fully separated.

An effective separate $\boldsymbol{\delta}_m$ of each slave node is calculated based on the components of the separation vector in equation 13 as:

$$\boldsymbol{\delta}_m = \sqrt{\langle \delta_n \rangle^2 + \delta_s^2 + \delta_t^2} \tag{16}$$

If the progression is a linear decay, the damage parameter then becomes:

$$D = 1 - \frac{\delta_m^{max} - \delta_m^0}{\delta_m^f - \delta_m^0} \tag{17}$$

The superscript *0* indicates the separation at the time that the adhesive interface strength is achieved at that node pair. The superscript *f* indicates the user-input material parameter (separation at failure) related to the damage evolution model, the maximum separation to failure. The superscript *max* indicates the maximum separation of the slave node from the master surface up to the current time during this progressive interface failure.

If the progression is an exponential decay, the damage parameter is defined as:

$$D = 1 - \frac{\delta_m^0}{\delta_m^{max}}\left(1 - \frac{1-exp\left(-\alpha\frac{\delta_m^{max}-\delta_m^0}{\delta_m^f-\delta_m^0}\right)}{1-exp(-\alpha)}\right) \tag{18}$$

where the exponent α is user-input material parameter.

The energy-based damage parameter uses a linear decay based on the change in the area under the traction separation curve. This is then compared to a user input maximum "fracture energy," *G,* such that:

$$D = \frac{\delta_m^f(\delta_m^{max}-\delta_m^0)}{\delta_m^{max}\left(\delta_m^f-\delta_m^0\right)} \tag{19}$$

where $\delta_m^f = 2G/T_{eff}^0$ and T_{eff}^0 is the effective traction at damage initiation, which is calculated following the effective separation in equation 16.

When separation is complete, the interface behavior can transition to a contact behavior. In Abaqus any contact formulation can be used that is allowable for the solver and element types employed. Contact behavior is simulated using a modification of the standard isotropic Coulomb friction model. In this model, the shear stresses on the contacting surface are combined to an effective shear stress as:

$$\tau_{crit} = \mu P \tag{20}$$

where μ is the friction coefficient and *P* is the normal pressure due to contact.

The motion is defined so that nodal shear stress no longer increases with increased nodal displacement beyond this critical shear stress. A penalty contact enforcement method is used. Normal contact can similarly be calculated between separated surfaces should they subsequently interact.

In LS-DYNA, the adhered surfaces were modeled using a "tiebreaker" function. In this function, nodes initially in contact are assumed to remain in contact, using a standard penalty formulation, until the damage initiation criterion is reached. The standard penalty formulation gives an interface stiffness approximately the same order of magnitude of the stiffness of the underlying master element. Therefore, unlike in Abaqus, a specific interface stiffness need not be defined.

The failure is initiated at each element based on the interface stress components when:

$$\left[\frac{|\sigma_n|}{\sigma_n^f}\right]^2 + \left[\frac{|\sigma_s|}{\sigma_s^f}\right]^2 \geq 1 \tag{21}$$

where the superscript *f* indicates the user-input interface adhesive strength and the subscripts *n* and *s* indicate the components in the normal and shear directions, respectively.

The damage progresses as a linear function of the distance between points that were initially in contact as:

$$\boldsymbol{\sigma} = (D)\boldsymbol{\sigma}_o \tag{22}$$

where the subscript *o* indicates the stress tensor at the time that the adhesive strength is reached.

The energy released due to the failure, *E,* at the interface can then be estimated as:

$$E = 0.5\ (\delta_{crit})\sqrt{\max(\sigma_n,\ 0)^2 + {\sigma_s}^2} \tag{23}$$

where δ_{crit} is the separation between the slave node and the master surface at the time when the separation between the slave node and the master surfaces reaches the user-input maximum separation distance to failure.

LS-DYNA uses a similar contact model based on Coulomb friction. The particular methods to identify, enforce, and control contact, while also penalty-based, vary in details from those used in the Abaqus software. See the respective documentation for further details (refs. 15 and 16).

These basic models were used and compared to predict the separation behavior between the Sylgard epoxy material and the aluminum metal material under a range of loading modes and magnitudes.

Quasi-static – Single Mode Loading

The prediction of the failure of the studied interfaces under single mode loads was first examined. These studies were based on those of Stevens (ref. 7), who used the Abaqus built-in cohesive interface model to predict experimentally measured tensile and shear separation forces of systems of aluminum plates adhered together by a thin adhesive layer of Sylgard. Qualitative comparisons will be made between the separation behavior predicted by this model and that of the Stevens' work. Quantitative comparisons are also made between the traction-separation curves under each loading mode found in this work and that of the referenced study (ref. 7).

Tensile Adhesive Strength

Tensile adhesive strength was examined using a system of two 15-mm tall, 16-mm radius cylindrical aluminum disks initially bonded over the entire area of the two facing circular surfaces with a 0.25-mm thick layer of the epoxy Sylgard. The system was modeled using the commercial code Abaqus version 2019. The material properties were as described previously. The interface model described previously was also used with a displacement-based exponential damage evolution model as in equation 18. The two adhered interfaces were given a normal stiffness of 210 GPa and a tangential stiffness of 420 GPa following the referenced work (ref. 7) and guidance from a work by Chung and Chaudhury (ref. 6). In reference 6, it was indicated that, for thin layers, the interface shear stiffness can be approximated as one hundred times the ratio of the shear modulus of the adhesive to the thickness of the adhesive layer and that normal stiffness of the interface bond can be approximated as half the shear stiffness. The maximum normal adhesive strength used was 0.44 MPa, and the maximum shear adhesive strength was 0.3 MPa, following the work of Stevens (ref. 7). The maximum displacement to failure $\delta_m^f$was 2 mm with an exponential decay parameter α of 4 (see eq. 18).

A one-quarter symmetry model was used in this study (fig. 1a). The bottom surface of the bottom disk was fully constrained. The top surface of the top disk was kinetically coupled to a single

node at the center of this disc (on the axes of symmetry), which was moved normal to the surface at a rate of 0.01 m/s. A quasi-static dynamic implicit analysis was performed with a constant timestep of 5e-7s. A constant timestep was used to control the rate of separation of the discs to be comparable to that of the cited experiment. With a constant displacement rate of the top surface for this the quasi-static analysis, the timestep controlled the rate of separation of the adhered interfaces. The reaction force at the control point node where this displacement rate was applied was tracked with each timestep.

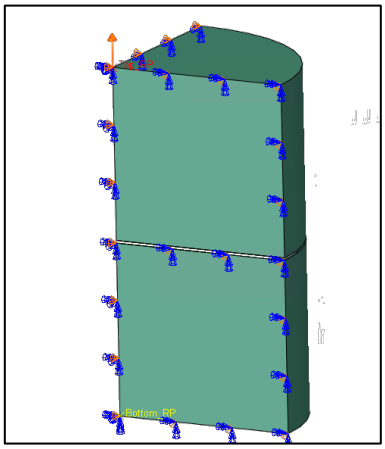

(a)
Model with boundary conditions and loads

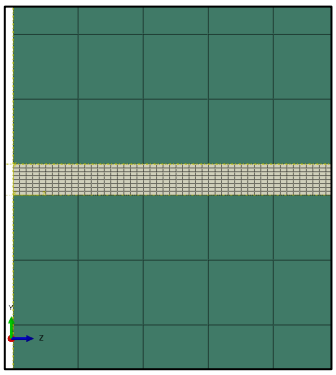

(b)
Mesh

Figure 1
Quasi-static tensile adhesive strength model

The aluminum disks were meshed with 500 micron linear three-dimensional hexahedral elements with reduced integration and hourglass control. The epoxy, which was made of the hyperelastic material, was meshed with 50 micron linear three-dimensional hexahedral elements with a hybrid formulation, reduced integration, and hourglass control per guidance from the Abaqus documentation for this material type (ref. 15). The mesh of the epoxy was an order of magnitude smaller than that of the metal disk, so that the behavior of the epoxy during the progressive failure of the interfaces with the aluminum plates could be well captured. With a mesh of 100 micron elements, comparable force-displacement behavior resulted, but the deformation of the epoxy layer during the separation was found to be somewhat different. As a result, the finer mesh was used in this study (see fig. 1b)

Shear Adhesive Strength

The shear adhesive strength was examined through a thin (0.25-mm) layer of epoxy bonding two long aluminum blocks with a square cross section of 100 mm^2 and a length of 70 mm. The same material properties as used in the tensile adhesive strength study were applied to this system. The same normal and shear adhesive strengths as the tensile study were also used here. However, the normal and shear cohesive interface stiffnesses were reduced by approximately 50% per the referenced paper (ref. 7) to 105 and 192 GPa. Following the previous work (ref. 7), an energy-based damage evolution model was employed in this shear strength simulation, with a failure energy of 50 N-m. After the surfaces separated, a sliding friction coefficient of 0.2 was to be applied.

The two aluminum blocks were constrained by L-brackets as in figure 2. The bottom bracket was constrained in all degrees of freedom. The top bracket was constrained in all degrees of freedom except in the direction of the shear force. The blocks were prevented from moving in the direction of their longest dimension. The left side of the top L-bracket was kinetically tied to a single node to which a constant displacement rate was applied. The fixed boundary condition on the right side of the bottom plate was similarly applied using a kinetically tied single node. A penalty function enforced contact method was applied to all interfaces between blocks and brackets, and a sliding friction coefficient of 0.2 was used. Following the referenced study (ref. 7), a small gap was left between the top of the top aluminum block and the top L-bracket to allow slight rotation of the block, facilitating separation. The size of the gap was adjusted to control the separation behavior. A quasi-static dynamic implicit analysis was performed. The reaction force at the constrained nodes was tracked at each iteration.

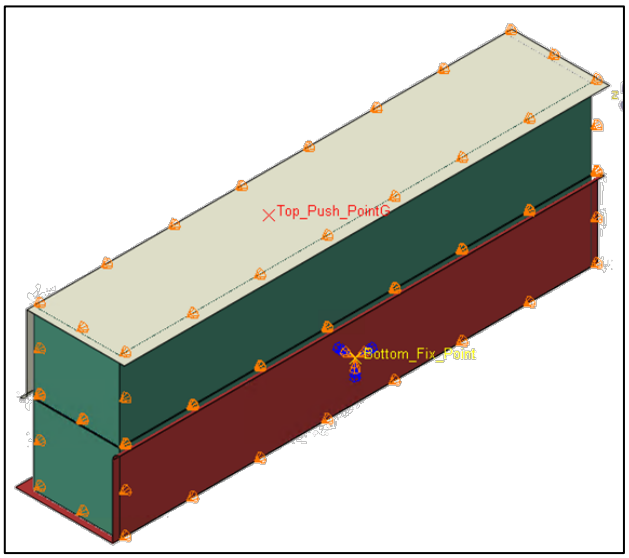

Figure 2
Quasi-static shear adhesive strength model

The aluminum blocks were meshed with 1-mm three-dimensional linear hexahedral elements with reduced integration formulation and hourglass control. The epoxy was meshed with 0.25 x 0.25 x 0.1-mm three-dimensional linear hexahedral elements with a constant pressure/hybrid formulation, reduced integration, and hourglass control. The brackets were modeled as discrete rigid shells.

Dynamic Loading

Next, the separation of adhered surfaces between the epoxy and metal materials was examined under dynamic conditions. The system used in this study represented an aluminum cylindrical canister that has two main regions. The larger region was nearly filled with the Sylgard epoxy except for a small gap space. The epoxy was initially fully bonded to the top and sides of the inner surfaces of the aluminum canister. The smaller region at the bottom was unfilled. A transient pressure load of the profile in figure 3a was applied to a bottom exterior surface of the canister as shown in figure 3b over a total duration of 8 ms. The amplitude of the pressure load was scaled to a peak pressure that was calculated so that the system was accelerated by a maximum of either 0.015, 0.17, or 8.25 kG. The system investigated in this dynamic was created so that the inner chamber of the canister had the same radius as the quasi-static tensile adhesive strength study and the same length as the quasi-static shear adhesive strength study.

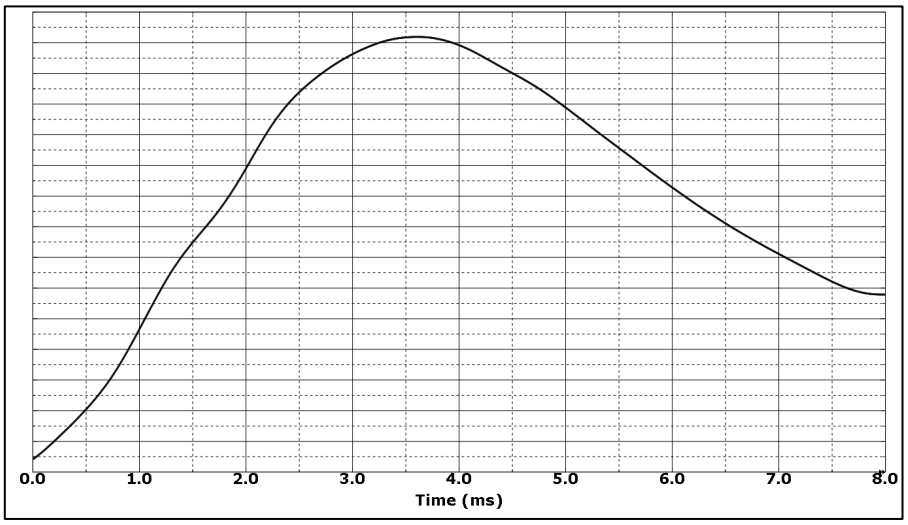

(a)
Dimensionless load profile

Figure 3
Model for comparative studies under dynamic loads

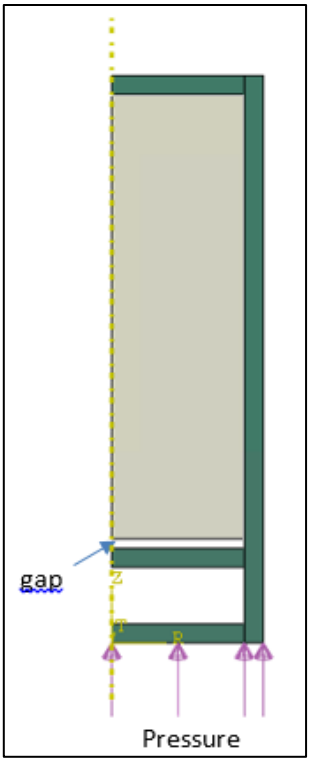

(b)
System model

Figure 3
(continued)

The system was represented with an axisymmetric approximation using 500-micron elements for the aluminum housing and 40+micron elements for the epoxy. Linear quadrilateral axisymmetric elements with a reduced integration formulation and hourglass control were used for each system component. An explicit solver was used for this transient analysis. The total contact force between the epoxy and the bottom surface of the main interior chamber of the canister was tracked at each timestep as a measure of the effect of the separation of the epoxy from the canister during the dynamic event. The bottom of the inner chamber containing the epoxy was created to be separate from the outer wall of the canister so that the applied pressure load did not directly affect the interaction of the epoxy and the canister wall. The stress distributions in the canister were also qualitatively studied.

The general interface model described previously was used. The adhesive strength was the same as in the quasi-static studies. The interface stiffness and damage evolution parameters were varied to examine their effects on the contact force as a result of the separation of the epoxy from the canister both in its magnitude and the timing of this impact. Once full separation occurred, the cohesive interface behavior was converted to a general contact model with a coefficient of sliding friction of 0.1. The system was also studied using a frictional interface contact model only, without adhesion, in order to assess the differences in the predicted behavior of the epoxy in the canister. The friction coefficient was varied from 0 to 0.9.

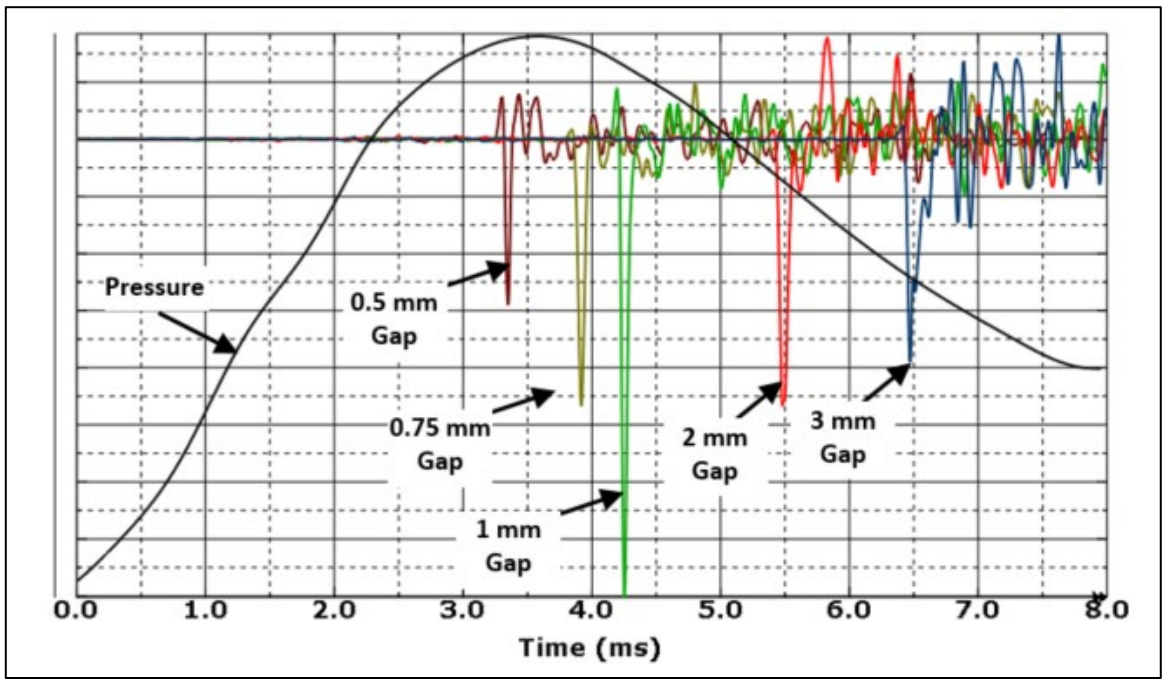

Figure 4
Effect of gap size on contact pressure between separated epoxy and base of canister

Previous work has suggested a number of ways to define the normal and tangential moduli of adhered interfaces, some of which include the effects of the area and thickness of the adhesive layer. The sensitivity of the model predictions was demonstrated, in part, in the two-fold differences in interface stiffness used in the referenced paper that was the basis of the quasi-static studies (ref. 7). While some studies (refs. 1, 5, and 6) have indicated that strain rate and thickness effects on interface stiffness become negligible as the thickness and material modulus of the adhesive increases, the relationships between material and interface stiffness are not well established, particularly under dynamic loads. As a result, the normal and shear stiffness of the adhesive interface were simply selected to be both equal to the bulk modulus of the Sylgard material for the next set of studies.

The system was evaluated using the two commercial codes Abaqus and LS-DYNA. A number of cases varying the interface model parameters and load were evaluated using Abaqus (table 1). For each of the three load magnitudes examined, an interface strength of 1, 10, and 100 kPa was evaluated. For the largest load and highest interface strength, the effect of the damage evolution model was examined, comparing the energy-based and displacement-based methods. The effect of the interface stiffness was also evaluated for this load and interface strength, with the stiffness reduced an order of magnitude. Finally, rather than a cohesive interface model, a frictional interface model was used, varying from frictionless to an interface friction coefficient of 0.9. The magnitude and timing of the maximum contact force between the epoxy and the bottom face of the canister were compared among all of these cases.

Table 1
Effect of interface model cases studied

Case	Maximum acceleration (kG)	Interface strength (kPa)	Damage evolution	Interface normal stiffness (GPa)	Friction coefficient	LS-DYNA model
1	0.015	1	Displacement/ Exponential	O(e9)	--	
2	0.17	1	Displacement/ Exponential	O(e9)	--	
3	8.25	1	Displacement/ Exponential	O(e9)	--	X
4	0.015	10	Displacement/ Exponential	O(e9)	--	
5	0.17	10	Displacement/ Exponential	O(e9)	--	
6	8.25	10	Displacement/ Exponential	O(e9)	--	X
7	0.015	100	Displacement/ Exponential	O(e9)	--	
8	0.17	100	Displacement/ Exponential	O(e9)	--	
9	8.25	100	Displacement/ Exponential	O(e9)	--	X
10	8.25	100	Energy	O(e9)	--	
11	8.25	100	Displacement/ Exponential	O(e8)	--	
12	8.25	--	--	--	0	X
13	8.25	--	--	--	0.1	
14	8.25	--	--	--	0.2	
15	8.25	--	--	--	0.3	
16	8.25	--	--	--	0.5	
17	8.25	--	--	--	0.7	
18	8.25	--	--	--	0.9	X

Note: LS-DYNA does not have an interface stiffness parameter. A linear displacement-based damage evolution with a maximum separation to complete failure was used.

A subset of these cases was evaluated using LS-DYNA (noted with an X in table 1). Because the damage evolution behavior was different for the built-in function of LS-DYNA, although a displacement-based model can be used, a series of studies were performed to select the model parameters that would produce a system behavior that corresponded to the behavior predicted for the displacement-based damage evolution model using the Abaqus built-in function. Comparisons were noted among cases and software, so general conclusions could be drawn regarding the behavior predicted with the various interface models, the sensitivity to the model parameters selected, - the loading conditions to which the system was subjected, and the influence of the commercial package used.

RESULTS

Using the three main systems described, the effects of the interface model and model parameters on the separation behavior of a metal-epoxy interface were examined. The quasi-static validations studies involving the single mode loading bond strength on an assembly of two aluminum plates held together by a thin layer of epoxy will first be discussed. Next, the studies of a cylindrical canister partially filled with a volume of epoxy bonded to the internal surfaces of the canister will be presented. Finally,he effects of the interface model parameters, the commercial software used, and a comparison to a contact-based friction interface model with no adhesion will be evaluated.

Validation Studies

To understand the effects of the interface model parameters on the prediction of the separation behavior between a metal and an epoxy, two validation studies were performed. In the first study, the tensile separation was examined under quasi-static conditions. In the second study, the shear separation was evaluated.

Tensile Adhesive Strength

In the simulations of the tensile adhesive strength, the model developed in this work was able to qualitatively predict the general sinusoidal “cavitation-like” failure behavior of an interface of a thin adhesive under tensile load that has been described in a number of experimental and computational models (refs. 6 and 7). Further, the tensile force to separation predicted by this model was within 20% of the experimentally predicted tensile force to separation for the same system that was presented in the published paper on which this validation study was based (ref. 7).

The “cavitation-like” interface failure behavior that has been described in the separation phenomena of thin adhesive “sandwiches” under tensile load results from local areas of separation that initially form within the interior of the areas of adhesion. These pillar-like structures then fail locally from the edges of their areas of contact. The pillars also stretch under the tensile load as they are pulled by their adhered surfaces to the moving and fixed aluminum plates. The interaction between the stiffness and the strength of the adhesive material itself is countered by the adhesive strength resulting in the patterns of failure seen. The distance between these pillars along a two-dimensional cross section has been shown to be a scalar multiple of the adhesive thickness (refs. 6 through 8). Figures 5a and 5b show the development of the pillar structures predicted by the current model. For this behavior to be simulated, a very fine mesh in the adhesive and a very small timestep are required. Figure 5c shows the damage parameter at the interface between the top aluminum plate and the adhesive. Red indicates fully separated, blue indicates full bonded. Notice that as the “pillar” thickness decreases, the stress at the adhered region, and therefore, the magnitude of the damage parameter, increases, until full separation occurs. The bands of common radial dimension and damage parameter in figure 5c correspond to the sinusoidal pattern of these pillar features in the two-dimensional axisymmetric model of Stevens (ref. 7) and the analytical models of Chung (ref. 6).

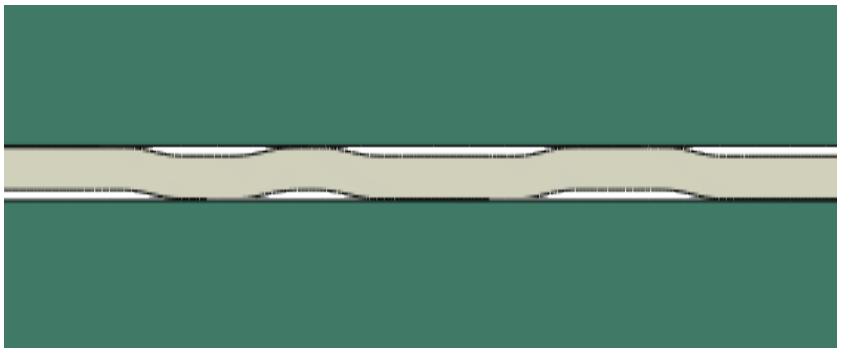

(a)
Separation of epoxy layer from aluminum plates

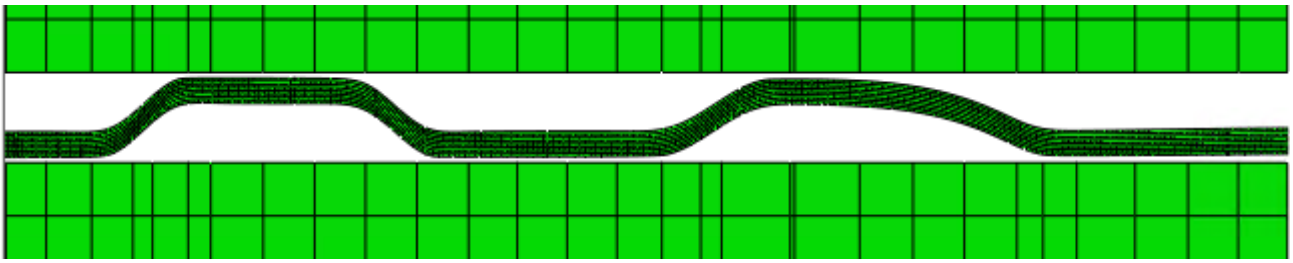

(b)
Mesh used to achieve this behavior

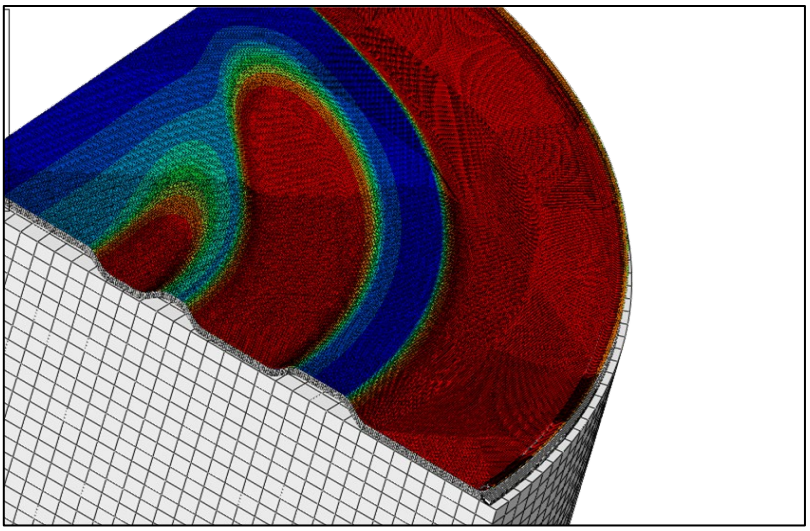

Note: Blue indicates fully bonded and red indicates fully separated.

(c)
Damage parameter in individual elements of top surface of epoxy during separation

Figure 5
Adhesive failure under tensile load

Figure 6 shows the force displacement curve for the load on the top plate. While the peak force well correlated to that predicted by the previous publication, the force during the evolution of the damage predicted in this model was different. This is likely due to the differences in the rate of

separation of the two aluminum plates, the material model of the epoxy, and the damage evolution model and parameters used in the two models. The previous publication varied these parameters until they were able to match the experimental data, but noted how there was large uncertainty in the "calibration of the traction separation model behavior" (ref. 7).

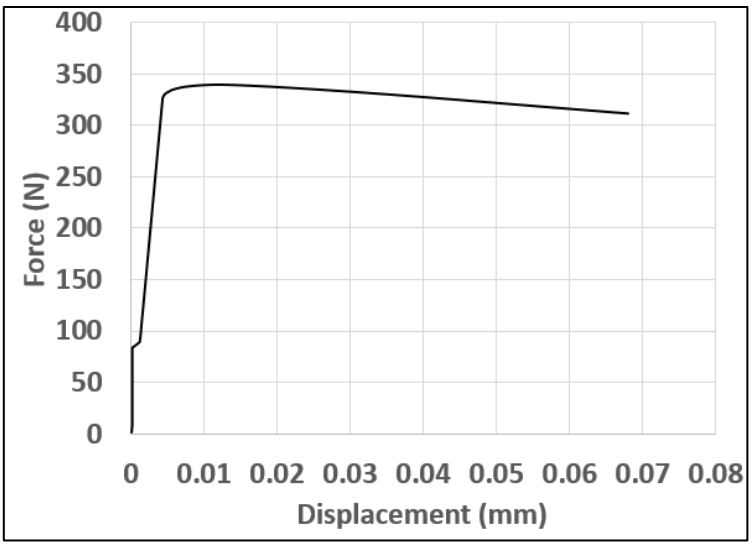

Figure 6
Traction-separation behavior for tensile adhesive strength model

The fine mesh and small timestep required to capture the physical separation phenomena resulted in a significant computational cost for properly simulating this interface separation behavior. Run times were on the order of days even using one 36-core, 256-GB node of a high performance computing network. The analysis was stopped after 72 hr even though full separation was not reached, since identifying the maximum force and the qualitative depiction of the separation behavior was the focus of the study.

Shear Adhesive Strength

Similar to the prediction of the tensile adhesive strength, the model used in the current work was able to qualitatively predict the separation behavior of a thin adhesive epoxy layer between two aluminum plates. Due to the very small timestep to ensure the behavior was captured and for numerical stability to ensure elements did not invert during the application of the shear force, only the initiation of the separation was simulated before the analysis was stopped. Under shear loading, the adhesive separated from the ends of the plates that were normal to the direction of the applied load (fig. 7). The timing, extent, and evolution of the separation were influenced by the cohesive interface and damage model parameters selected, the mesh of the adhesive, and the dimensions of the "fixture" used to apply the load. Following the previous publication, a slight rotation of the top plate was allowed during the shear loading to induce a slight tensile load on the edge of the interface and initiate separation. The predicted behavior was very sensitive to the amount of rotation of the top block, which was controlled by the size of the gap between the block and the top of the fixture bracket. This relationship was also noted in reference 7.

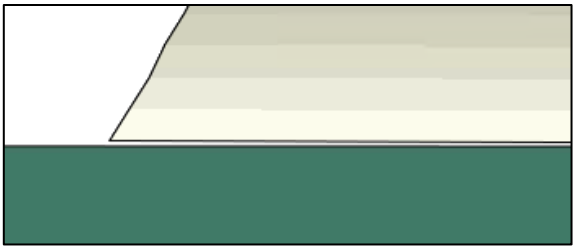

(a)
Initiation of separation under shear loading

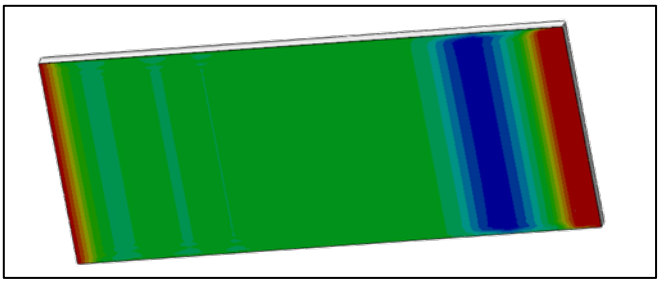

Note: Blue indicates fully bonded and red indicates fully separated.

(b)
Damage parameter of individual elements on bottom surface of epoxy at initiation of separation under shear load

Figure 7
Adhesive failure under shear loads

From these validation studies, it was found that the general phenomena of the separation behavior of thin adhesive epoxy layers between two metal plates under pure tensile and pure shear loads could be simulated using the models in this work. Additionally, the model could well approximate the maximum force required to cause this separation. The actual transient changes in this force, however, and slopes of load-displacement curves were found to be very sensitive to the cohesive interface damage evolution model, material properties, mesh and load rate used as well as to the effects induced by the system components through which the load was applied. The long run times, due to the fine mesh and small timestep, required to capture the small transient changes in the shape of the adhesive layer and extent of interface bonding during the separation phenomenon would likely make the use of this modeling method infeasible when examining the separation of adhered surfaces within large systems with many components.

In large systems, the interface behavior is included in a model to predict the interactions between system components and estimate the changes in the load transferred through these interfaces within the structure over time. As such, capturing the details of the separation behavior are less important than capturing the timing of the separation, the energy released during the separation, and the movement of the components during and after separation. The next series of studies investigated the sensitivity of these behaviors to cohesive interface model parameters and compares the prediction of the interactions with a cohesive model to those using a frictional interface model. Comparisons were quantitatively made using the contact force between the internal bottom surface of the canister and the epoxy after separation (table 2). The effect on the stresses induced in the system and the separation behavior will be discussed.

Table 2
Maximum contact force magnitude and time of contact for different interface models

Case	Maximum contact force (N)	Time of maximum impact force (ms)
1	236.8	5.14
2	690.5	1.93
3	1238.0	1.15
3 Dyna	1271.9	1.14
4	0	--
5	748.7	2.79
6	1193.0	1.31
6 Dyna	1272	1.14
7	0	--
8	0	--
9	6.9	2.55
9 Dyna	1.9	3.48
10	6.7	2.22
11	0.2	2.95
12	1334.0	1.14
12 Dyna	1271.8	1.14
13	1324.5	1.14
14	1320.2	1.14
15	1316.4	1.14
16	1309.3	1.14
17	1305.2	1.14
18	1305.2	1.14
18 Dyna	1223.6	1.14

Effect of Interface Strength

The interface strength controlled whether or not the epoxy separated from the aluminum canister and, if it separated, the time of this separation. Differences in timing of the separation during the applied load influenced the magnitude of the peak contact force, though the effect on the timing was more significant. The extent of the influence of the magnitude of the interface strength was controlled by the intensity of the applied load. For the smallest acceleration studied (0.015 kG), only the weakest interface (1 kPa) separated. For the largest acceleration studied (8.25 kG), the strongest interface (100 kPa) did not separate. However, for this large acceleration between the weak interface (1 kPa) and the moderate strength interface (10 kPa) with separation, the difference in the maximum contact force magnitude was less than 5%, and the difference in the timing of the contact was approximately 10%. For the intermediate acceleration studied (0.17 kG), the interface strength had a more significant effect, with a difference in magnitude of contact of more than 10% and a difference in the timing of the event of nearly 50%. Figures 8 through 10 show the differences in the contact force, damage parameter, and stress distributions at a common time, typically the time that the last case to separate contacted the base of the canister.

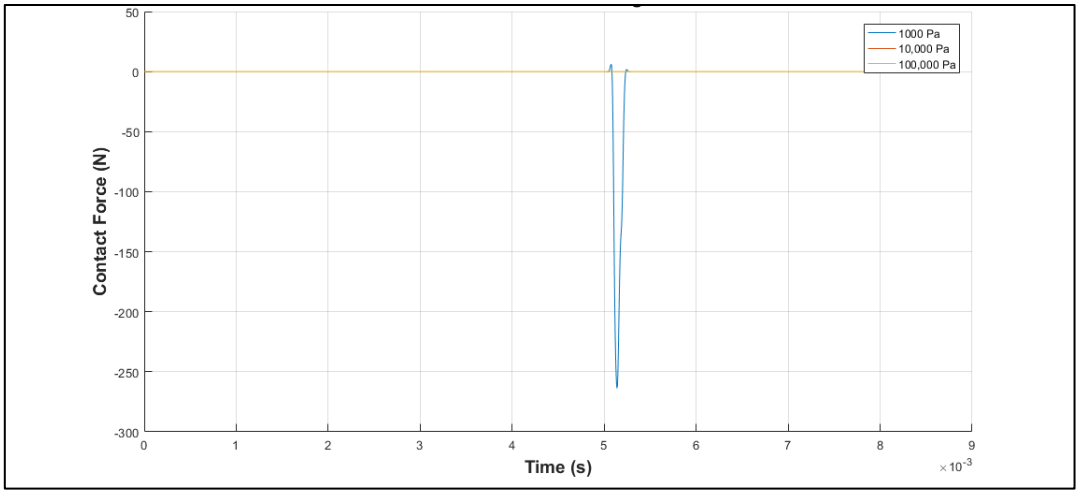

(a)
Contact force

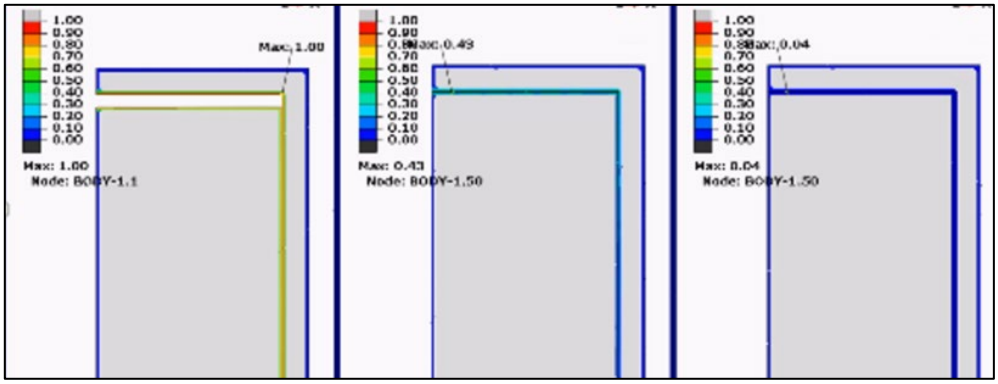

(b)
Damage parameter at 5.2 ms

Figure 8
Effect of interface strength under low-acceleration load case (0.015 kG)

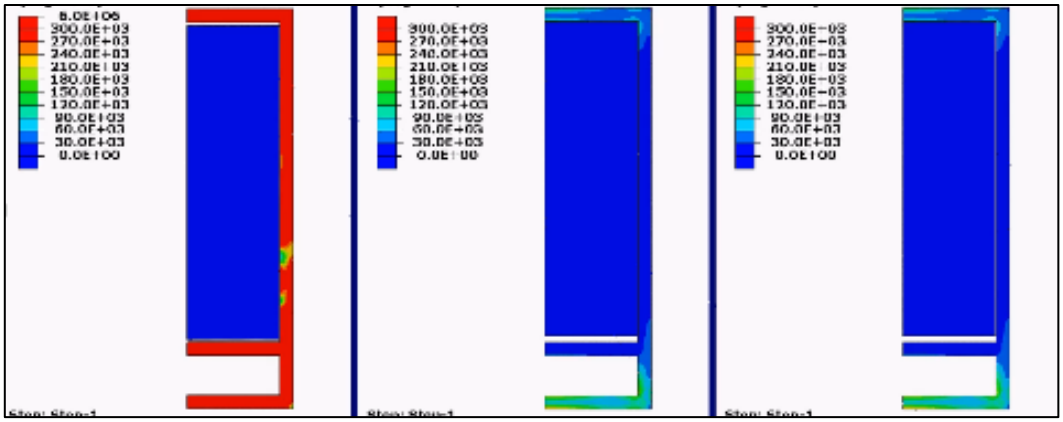

1 kPa 10 kPa 100 kPa

Note: Red is 0.3 MPa.

(c)
von Mises stress at 6.4 ms

Figure 8
(continued)

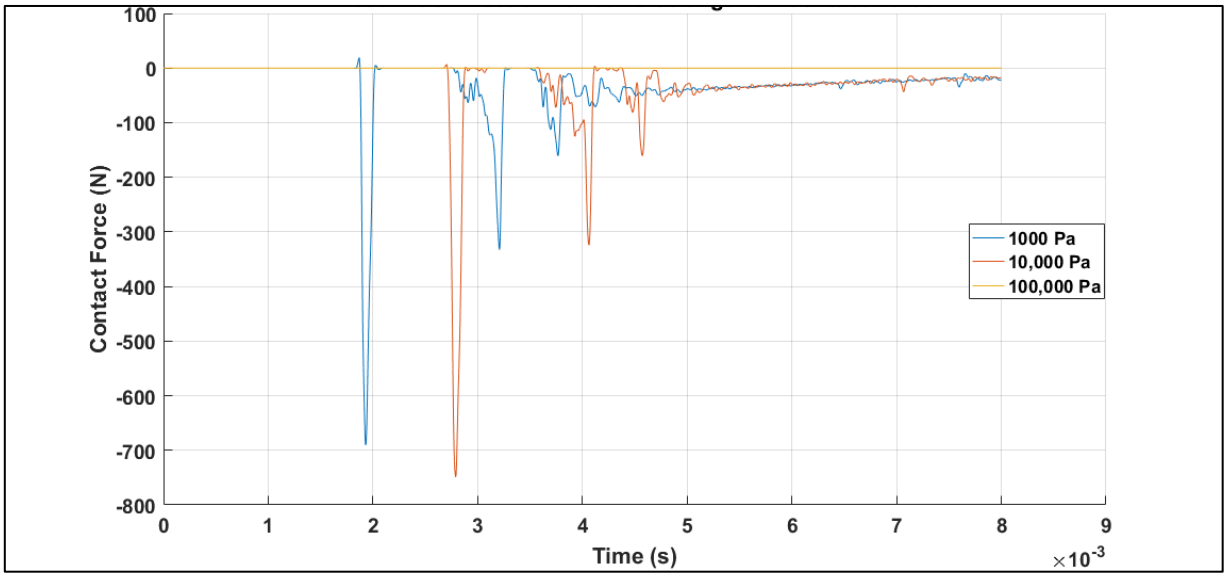

(a)
Contact force

Figure 9
Effect of interface strength under moderate-acceleration load case (0.17 kG)

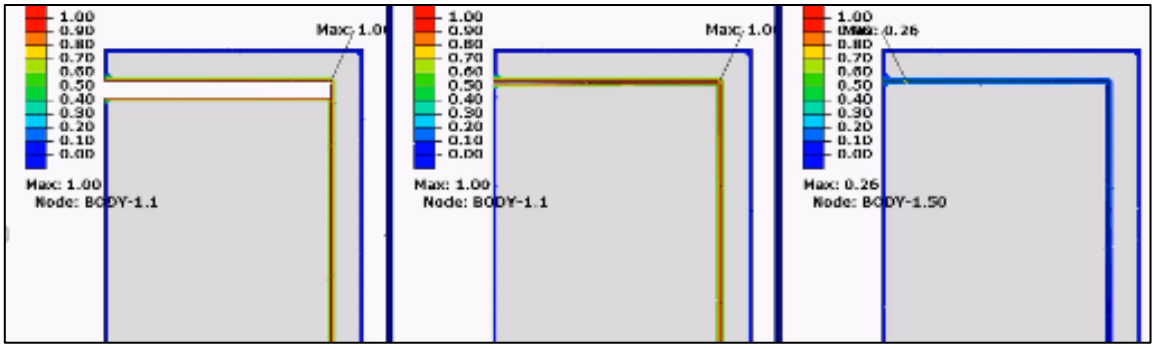

1 kPa 10 kPa 100 kPa

(b)
Damage parameter at 1.9 ms

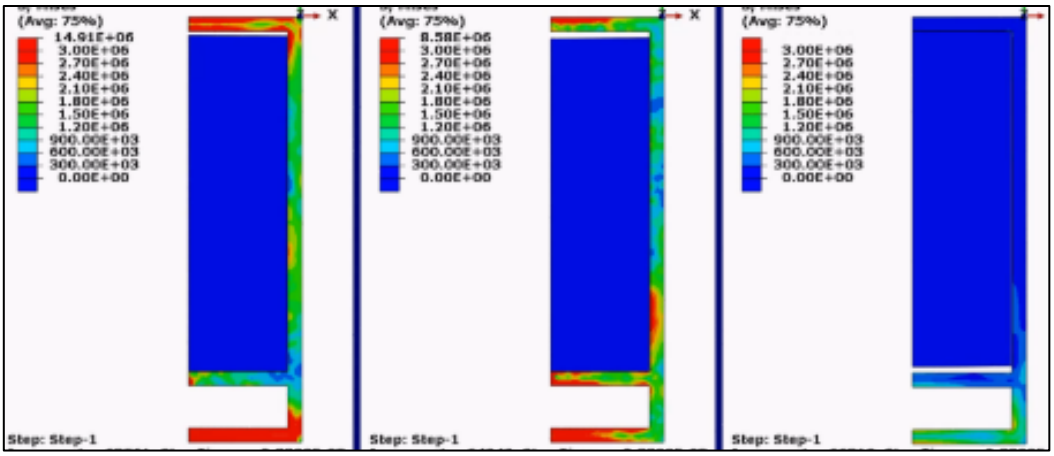

1 kPa 10 kPa 100 kPa

Note: Red is 3.0 MPa.

(c)
von Mises stress at 2.9 ms

Figure 9
(continued)

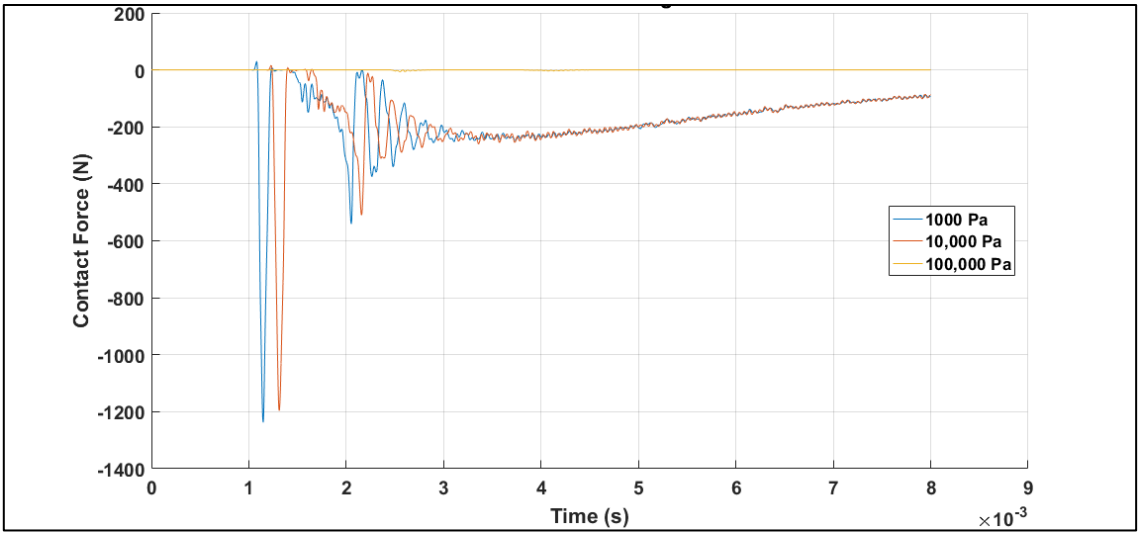

(a)
Contact force

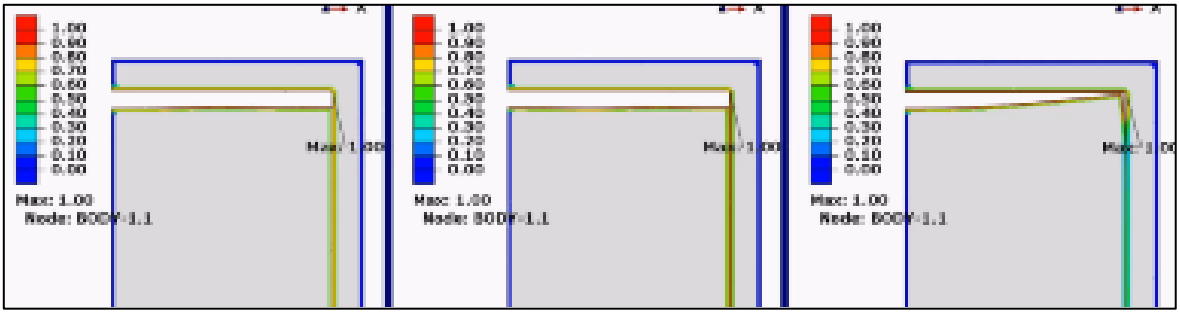

1 kPa 10 kPa 100 kPa

(b)
Damage parameter at 2.0 ms

Figure 10
Effect of interface strength under moderate-acceleration load case (8.5 kG)

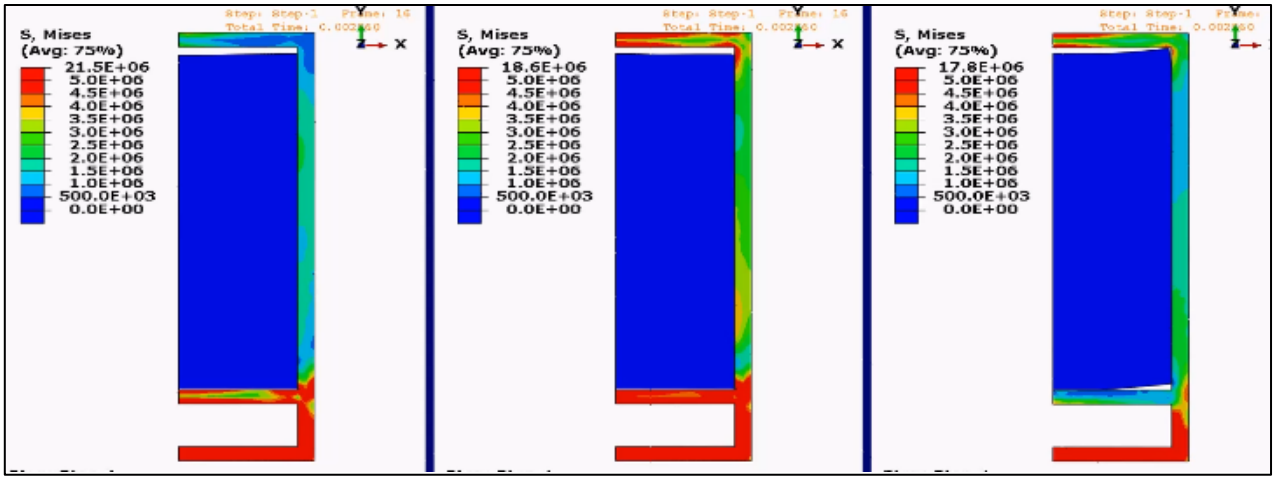

1 kPa 10 kPa 100 kPa

Note: Red is 5.0 MPa.

(c)
von Mises stress at 2.6 ms

Figure 10
(continued)

Comparison between Commercial Packages

For the same interface strength and load, the built-in functions of Abaqus and LS-DYNA both predicted comparable timing of separation and magnitude of resulting contact force with the proper selection of interface damage evolution model parameters (fig. 11). Differences in the magnitude of the peak contact force were due to the differences in the number of output points and the short duration, large magnitude load of the initial contact. Differences in later oscillations were due to the energy dissipation, contact formulation for the sliding after separation, material model, and element formulation. For a more direct comparison, a user defined cohesive interface model or material model can be written in either software to ensure the same model is applied in each software.

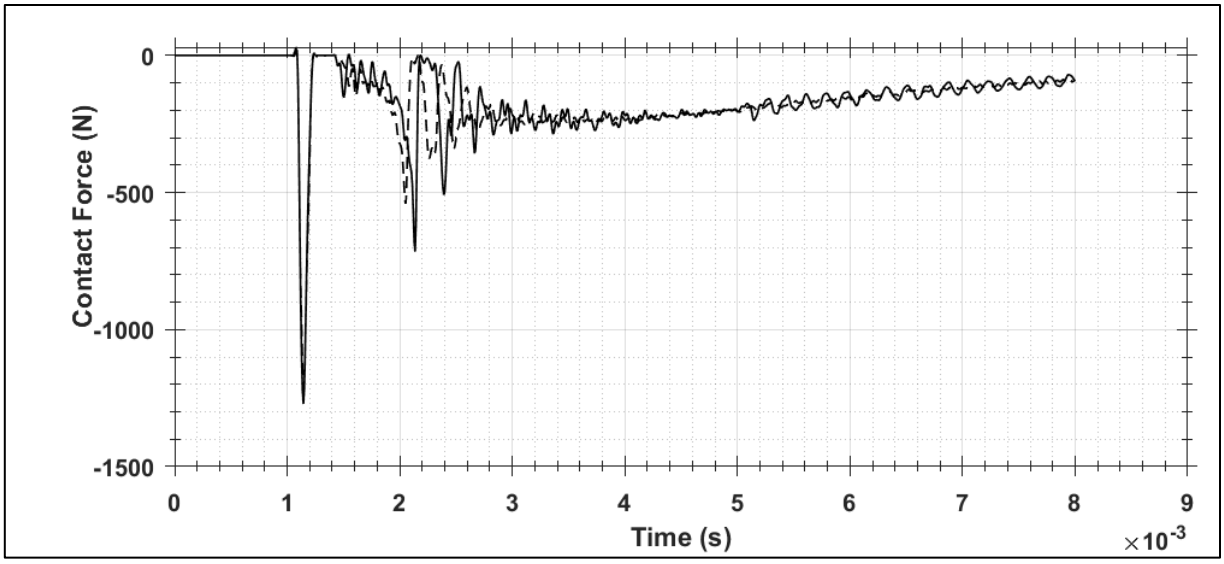

Figure 11
Contact force prediction for high-acceleration, low-interface strength case with LS-DYNA (solid line) and Abaqus (dashed line) built-in cohesive interface models

Effect of Interface Damage Model

The interface stiffness had a greater effect than did the damage evolution model used with the built-in functions of Abaqus (fig. 12). As the stiffness decreases, separation can be prevented for the same load and interface strength. This is because energy is put into stretching the interface, reducing the forces at the adhered nodes. In LS-DYNA, this same effect can be achieved through modification of the maximum separation to failure, where a very short separation to failure results in a quick separation and a large contact force upon impact, such as a stiff interface would, while a large separation to failure can prevent full separation of the interface, such as a more compliant interface would (fig. 13). By altering these parameters in these two software, comparable behavior could be achieved even without full separation (fig. 14). In the cases presented, the behaviors are slightly different, with the timing of the main impact and resulting subsequent impacts varying. However, the magnitude of the contact force in all cases is less than 10 N, and its effect on system behavior is, therefore, small compared to the approximately 1,000-N contact force that occurs with full separation of the epoxy. Therefore, the system response is less sensitive to the exact value of the stiffness parameter than it is to the order of magnitude of this value. Thus, all that is needed is the selection of a value that is small enough to reduce interface stresses, and therefore damage to the interface and separation, if such a behavior is expected.

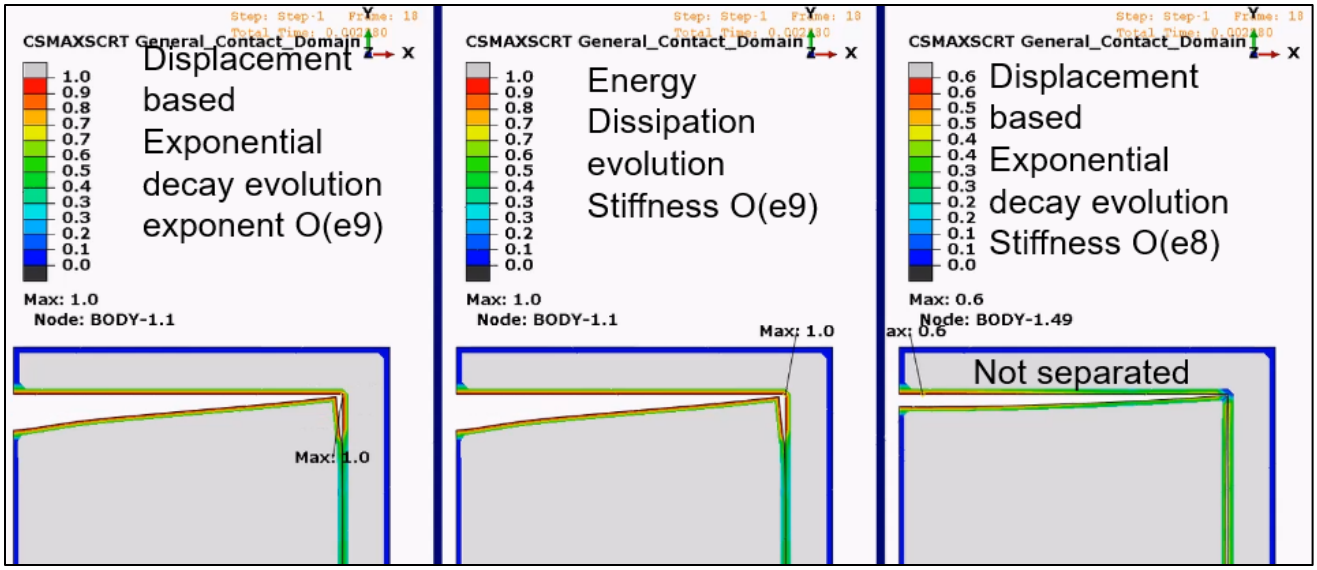

Figure 12
Effect of damage evolution model in Abaqus on separation behavior for high-acceleration, high-interface strength case

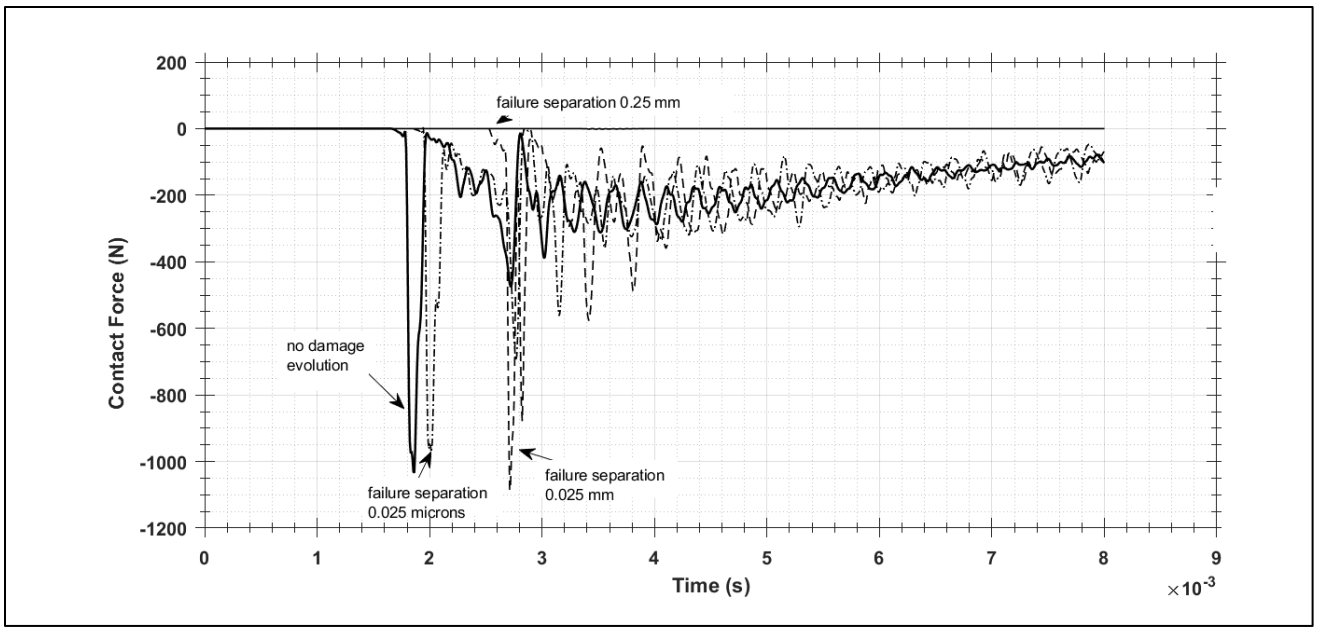

Figure 13
Effect of damage evolution parameter, maximum separation to failure, in LS-DYNA for high-acceleration, low-interface strength case

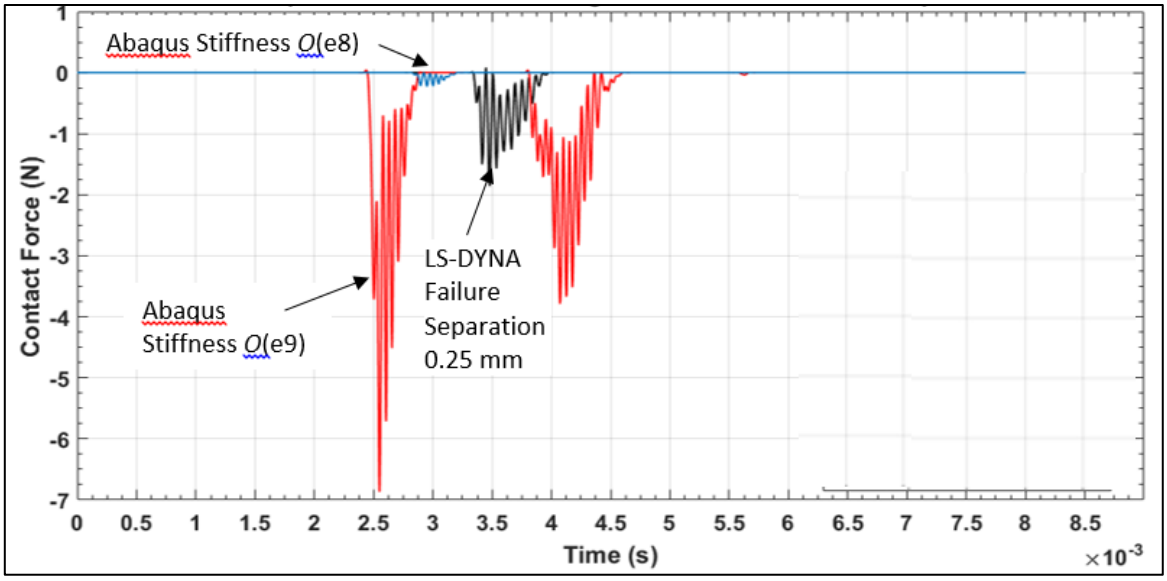

Figure 14
Contact force for various “interface stiffnesses” using Abaqus and LS-DYNA for high-acceleration, high-interface strength case

Comparison of Cohesive Interface to Friction

For a large ratio of applied load to interface strength, the cohesive interface model did not significantly alter the timing and magnitude of the maximum contact force. There was less than a 1% difference in the maximum contact force after separation that is predicted with a friction coefficient of 0.9 between that predicted with a cohesion model with an interface strength of 1 kPa and that predicted with a frictionless interface. The cases that included a cohesive interface model did somewhat reduce the amplitude of the subsequent oscillations of the contact force due to the dissipation of some energy imparted on the system during the separation of the initially adhered interface (fig. 15).

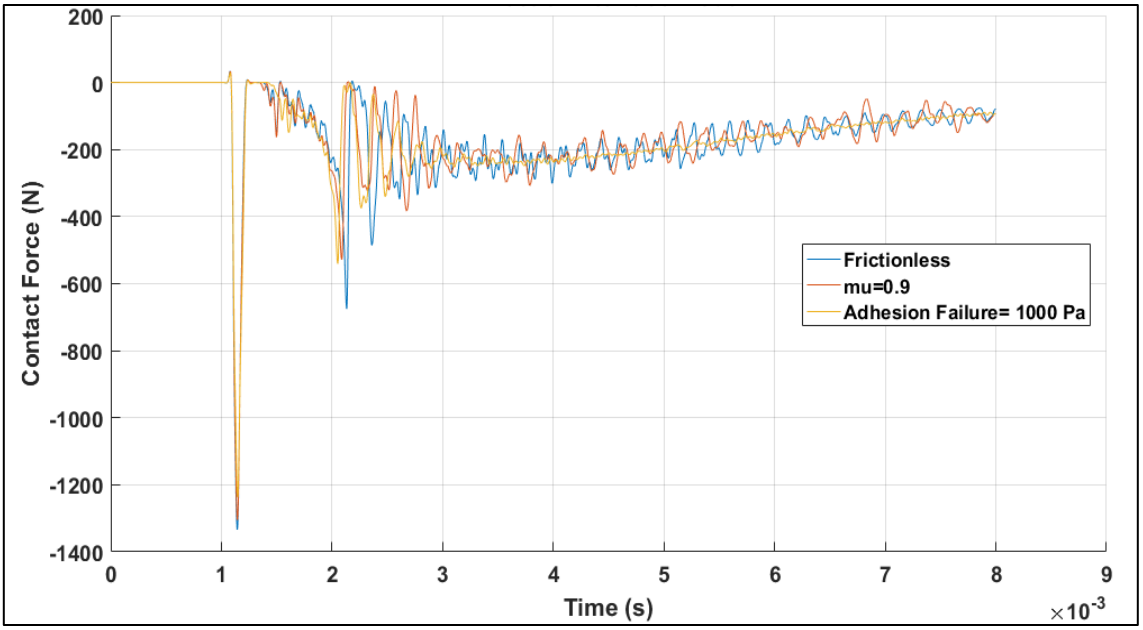

Figure 15
Comparison of cohesive interface and frictional interface models for high-acceleration, low-interface strength case

For the high-acceleration case, 8.5 kG, the value of the friction coefficient did not significantly affect the interaction between the epoxy and aluminum housing, with the maximum contact force magnitude varying approximately 2% among all cases from frictionless to a coefficient of 0.9 (fig. 16). The timing of the maximum impact increased slightly (less than 1%) with increases in the friction coefficient. As the acceleration load becomes smaller, the effect of the friction coefficient increases. For example, in the low-acceleration case (0.015 kG) in figure 17, the difference between the maximum force magnitude and timing becomes more significant for a case with a sufficiently small acceleration. In this case, for friction coefficients of 0.3 or more, either the epoxy did not separate at all or the distance that it did move was not enough for it to contact the base of the canister. Similarly, if there was an increased radial force between the epoxy and the wall, such as if the system was subjected to a rotational load, the effect of the frictional interface characteristics used would also likely increase. The extent of the increase would depend on the relative difference between the applied load and the load induced at the interface.

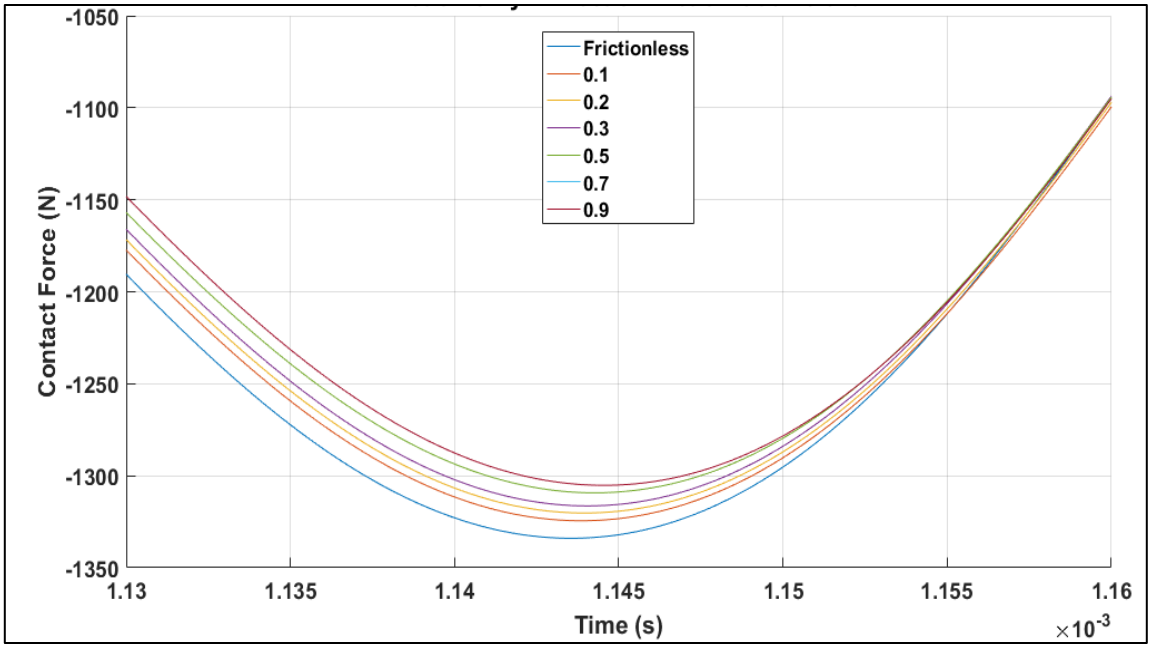

Figure 16
Effect of friction coefficient on maximum contact force for frictional interface only model high-acceleration case

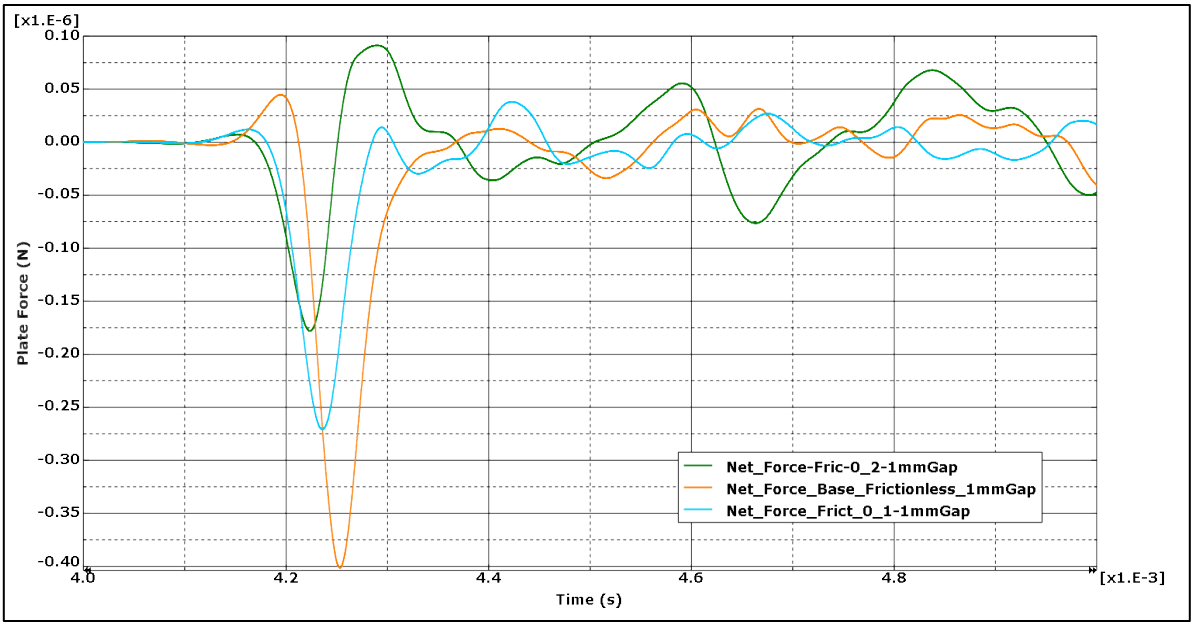

Figure 17
Effect of friction coefficient on maximum contact force for frictional interface only model low-acceleration case

Comparisons of Three-dimensional to Two-dimensional Simplifications

The failure of an adhered interface using the cohesive surface interaction model works by examining the local interface stress/displacement conditions of each element and removing individual pairs of nodes from the “surface interaction” set as the stresses or displacement at the interface between these nodes exceed the failure criterion. This creates a progressive separation during which the damage parameter value may not be continuous over the surface. As such, models that include cohesive interface interactions are more sensitive to the mesh quality and size. Of note are the differences between a two-dimensional or axisymmetric representation and a three-dimensional representation. The mesh and numerical problem formulation of the three-dimensional representation results in greater variations in stresses at the interface than an axisymmetric simplification of the system, even if the system geometry and load is “axisymmetric.” With the greater number of elements and greater range of stress variations, the time to full separation was longer for the three-dimensional model than for the axisymmetric model (fig. 18). Additionally, the contact force once the epoxy separates from the housing and impacts the base of the canister is smaller with the three-dimensional model due both to the change in timing of the impact load and the increased energy dissipation due to the progressive interface failure. This dependency on the model simplification is not present in the cases where a frictional interface model is used.

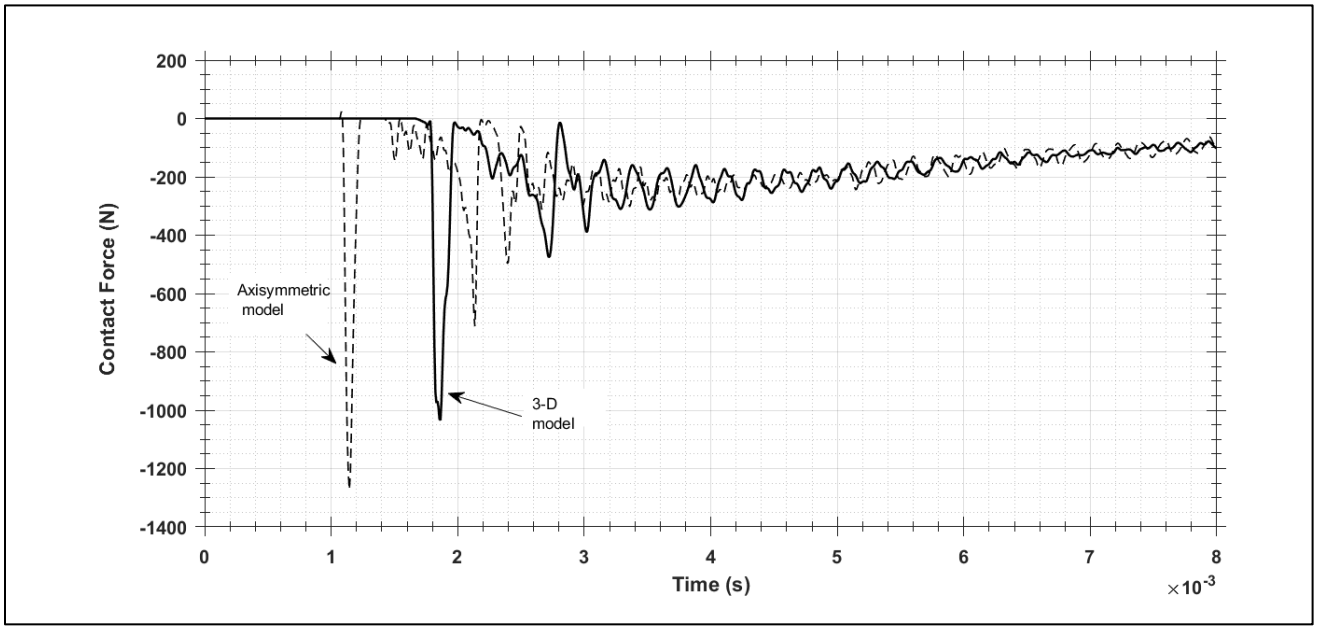

Figure 18
Effect of dimensional simplification on prediction of separation behavior high-acceleration, low-interface strength case

DISCUSSION

The work demonstrated the suitability of the use of built-in cohesive interface models from common finite element commercial codes to predict the time-dependent separation of an epoxy adhesive from an aluminum substrate. Sensitivities of these predictions to the model assumptions and the values of the parameters of the interface model and materials themselves were identified.

General separation mechanisms under tensile and shear loads could be simulated using a direct representation of the epoxy adhesive (hyperelastic material model) in addition to a cohesive interface model representing its bond interaction with the aluminum substrate. However, the accuracy of the predicted relationships between the separation force, displacement, and time were very sensitive to the interface model parameters (material interface properties), mesh used, and level of detail known about the system, including adhesive the layer thickness and rate of load application. It was found that similar behaviors and load histories could be predicted using different combinations of interface and material model behaviors. This could complicate the determination of which parameters are most important for a given model or system studied and limits the understanding of the physical system through the relationships between these seemingly physics-based parameters. Further, accurately capturing the physical transient behavior of the failing interface can be computationally intensive, limiting the application of the inclusion of a direct representation of thin adhesive layers into large system models. The study of the dynamic behavior of a system with a large mass of epoxy (adhesive) bonded to a metal substrate is a more feasible application for the inclusion of both the direct material model representation of the epoxy and the numerical interface model representation of the cohesive interface behavior.

The use of a cohesive interface model (cohesive zone model) was not found to add any more computational cost than a more standard contact or frictional interface model. In the study of large systems, the level of detail of the interface model can vary based on the particular system and conditions studied as well as the study intent. The influence of the interface model can then be assessed. This study found some general trends that can be used in selecting the interface model and parameters to be used for different situations. If the ratio of the system load to interface strength is relatively high, any cohesion mode or any level of friction coefficient could be used with little effect on the timing of the separation and the subsequent motion of the separated pieces. As this ratio becomes small, separation is unlikely, so a fully bonded interface approximation could even be suitable, reducing the computational resources required. If the components are already separated, then the system behavior is more sensitive to the friction coefficient used, and a better characterization of the frictional interface behavior may be required. If the applied load is moderate, and separation is possible, then the system behavior is more sensitive to the adhesive interface strength. Therefore, preliminary computational studies should be performed to understand the specific sensitivity, or experimental studies should be performed to better characterize the interface behavior.

For the cases studied, the damage evolution model used did not significantly influence the predicted behavior, timing of separation, or force transmitted due to separation if a separate interface stiffness parameter is chosen for the model as in Abaqus. If no interface stiffness is explicitly specified in the interface model, it can be implicitly applied to the model through the selection of the maximum separation to failure parameters that define a linear, displacement-based damage evolution model. It should be noted that if both the linear displacement-based damage model and the interface stiffness are used, they act like a pair of springs in series to lengthen the time to separation and reduce the interface stresses. Finally, caution should be used when coupling axisymmetric or other two-dimensional simplifications with cohesive interface models if accuracy of solution is more of an interest than comparative studies.

The insights gained in this work can help reduce the uncertainty related to assumptions made in representing initially bonded interfaces that may separate under dynamic loads so that better predictions of system behavior may be produced. This can also reduce study time as the number of model variations made to understand this uncertainty can be limited. Further insight may be gained through studying the effect of geometric scale on the trends identified in this work and as the span of applied loads, interface strengths, and properties of the bonded materials increases. Recent studies have indicated that the adhesive strength of epoxy metal interfaces may change with loading rate (ref. 18) so incorporating this rate-dependent interface strength may improve model predictions.

CONCLUSIONS

The work performed in the current study examined the use of built-in cohesive interface models to study the transient motion of initially adhered interfaces. The benefits, limitations, and applicability of these types of interface models were identified, particularly in comparison to simpler friction-based interface models. The implementation of the methods examined in this work can aid in improving the understanding of the physical phenomena at adhered interfaces, leading to better system design. The work can be expanded to investigate the use of cohesive zone models to explore means to tailor adhesive bonding and separation for both smooth and textured surfaces.

REFERENCES

1. Pinto, A. M. G., Campilho, R. D. S. G., Mendes, I. R., and Baptista, A. P. M., "Numerical and Experimental Analysis of Balanced and Unbalanced Adhesive Single-Lap Joints between Aluminum Adherands," The Journal of Adhesion, Vol. 90, No. 1, pp. 89-103, 2014.

2. Campilho, R. D. S. G. and Fernandes, T. A. B., "Comparative Evaluation of Single-lap Joints Bonded with Different Adhesives by Cohesive Zone Modelling," Procedia Engineering, Vol. 114, pp. 102-109, 2015.

3. Stuparu, F. A., Apostol, A., Constantinescu, D. H., Picu, C. R., Dandu, M., and Sorohan, S., "Cohesive and XFEM evaluation of adhesive failure for dissimilar single-lap joints," Procedia Structural Integrity, Vol. 2, pp. 316-325, 2016.

4. Andrews, E. H. and King, N. E., "Adhesion of Epoxy Resins to Metals Part 1," Journal of Material Science, Vol. 11, pp. 2004-2014, 1976.

5. Kim, J-S., Chisholm, B. J., and Bahr, J., "Adhesion study of silicone coatings: the interaction of thickness, modulus and shear rate on adhesion force," Biofouling, Vol. 23, No. 2, pp. 113-120.

6. Chung, J-Y. and Chaudhury, M. K., "Soft and Hard Adhesion," The Journal of Adhesion, Vol. 81. No. 10-11, pp. 1119-1145, 2005.

7. Stevens, R. R., "Modeling of Sylgard Adhesive Strength," Technical Report LA-UR-15-20757, Los Alamos National Laboratory, Los Alamos, NM, 3 February 2015.

8. Stevens, R. R., "Two models of Adhesive Debonding of Sylgard," Technical Report LA-UR-17-22150, Los Alamos National Laboratory, Los Alamos, NM, 14 March 2017.

9. Huang, G-Y. and Yan, J-F., "A mechanical model for the adhesive contact with local sliding induced by a tangential force," Acta Mechanica Solida Sinca, Vol. 30, pp. 369-373, August 2017.

10. Huo, J., Zhang, X., Yang, J., and Xiao, Y., "Experimental study on dynamic behavior of CFRP-to-steel interface," Structures, Vol. 20, pp. 465-47, August 2019.

11. Huntington-Thresher, W., Church, P. D., Kosecki, A., Gower, B., Proud, W. G., and Chapman, D., "Response of PBXs and Inert Substitutes in Launch and Impact Scenarios," Journal de Physique IV (Proceedings), Vol. 134, No. 1, pp. 231-236, August 2006.

12. Church, P., Huntington-Thresher, W., and Herdman, C., "Experimental and Simulation Analysis of Setback in Gun Launch," 19th International Symposium of Ballistics, Interlaken, Switzerland, 7 through 11 May 2001.

13. Espinosa, H. D., Dwivedi, S., and Lu, H-C., "Modeling impact induced delamination of woven fiber reinforced composites with contact/cohesive laws," Computer Methods in Applied Mechanical Engineering, Vol. 183, No. 3-4, pp. 259-290, March 2000.

14. Sauer, R. A., "A Survey of Computational Models for Adhesion," The Journal of Adhesion, Vol. 92, No. 2, pp. 81-120, 2016.

15. Dassault Systems, "ABAQUS 2019 Analysis User's Guide," Section 22.5.1 "Hyperelastic behavior of rubberlike materials".

REFERENCES
(continued)

16. Livermore Software Technology Center (LSTC), "2018 LS-DYNA R10113 Theory Manual," Chapter 22 Material Models Section 22.27 "Material 27: Incompressible Mooney-Rivlin Rubber", Livermore, CA.

17. Holzapfel, G. A., Nonlinear Solid Mechanics: A Continuum Approach for Engineering, John Wiley and Sons, New York, NY, 2000.

18. Saito, Y., Sudo, K., Kanamori, K., and Yonezu, A., Dynamic and Static Fracture Toughness of Aluminum-Epoxy Resin Interface, Paper 11081, 2019 American Society of Mechanical Engineers International Mechanical Engineering Congress and Exhibition, Salt Lake City, UT, 10 through 14 November 2019.

DISTRIBUTION LIST

U.S. Army DEVCOM AC
ATTN: FCDD-ACE-K
FCDD-ACM-AA, C. Florio
R. Lee
E. Bauer
FCDD-ACE-SA, L. Buckley
Picatinny Arsenal, NJ 07806-5000

Defense Technical Information Center (DTIC)
ATTN: Accessions Division
8725 John J. Kingman Road, Ste 0944
Fort Belvoir, VA 22060-6218

GIDEP Operations Center
P.O. Box 8000
Corona, CA 91718-8000
gidep@gidep.org

REVIEW AND APPROVAL OF ARDEC REPORTS

THIS IS A:

[X] **TECHNICAL REPORT** [ ] **SPECIAL REPORT**

[ ] **MEMORANDUM REPORT** [ ] **ARMAMENT GRADUATE SCHOOL REPORT**

FUNDING SOURCE CCDC AC Modeling and Simulation Strategic Advisory Group

[e.g., TEX3; 6.1 (ILIR, FTAS); 6.2; 6.3; PM funded EMD; PM funded Production/ESIP; Other (please identify)]

Modeling the Adhesion of Epoxy to Aluminum and their separation under Dynamic Loads using Abaqus and LS-DYNA
Title

Modeling and Simulation Advanced Initiatives Project
Project

Catherine S. Florio
Author/Project Engineer

Report number/Date received (to be completed by LCSD)

(973)724-8287
Extension

84, Second Floor
Building

FCDD-ACM-AA
Author's Office Symbol

PART 1. Must be signed before the report can be edited.

a. The draft copy of this report has been reviewed for technical accuracy and is approved for editing.

b. Use Distribution Statement A[X], B[ ], C[ ], D[ ], E[ ], or F[ ] for the reason checked on the continuation of this form. Reason: _____

1. If Statement A is selected, the report will be released to the National Technical Information Service (NTIS) for sale to the general public. Only unclassified reports whose distribution is not limited or controlled in any way are released to NTIS.

2. If Statement B, C, D, E, or F is selected, the report will be released to the Defense Technical Information Center (DTIC) which will limit distribution according to the conditions indicated in the statement.

c. The distribution list for this report has been reviewed for accuracy and completeness.

Edward Bauer
Division Chief (Date)

PART 2. To be signed either when draft report is submitted or after review of reproduction copy.

This report is approved for publication.

Edward Bauer
Division Chief (Date)

RDAR-CIS (Date)

LCSD 49 (1 Sept 16)
Supersedes SMCAR Form 49, 20 Dec 06